BSPN66720-12194-2

Remote Sensing Surveillance System for Supporting Illegal, Unreported and Unregulated (IUU) Fishing Control Activities

Republic of Korea
Pacific Islands

Project Completion Report

Submission Date: March 18th, 2020

Donors:

Ministry of Foreign Affairs

PACIFIC ISLANDS FORUM SECRETARIAT

Implementing Agencies:

KIOST

Table of Contents

Acronyms and Abbreviations

APEC	Asia-Pacific Economic Cooperation
CROP	Council of Regional Organisations in the Pacific
ESA	European Space Agency
PICT	Pacific Island Countries and Territories
PIFS	Pacific Island Forum Secretariat
ROK	Republic of Korea
ROK-PI-IUU	Republic of Korea-Pacific Islands Remote Sensing Surveillance System for Supporting Illegal, Unreported and Unregulated (IUU) Fishing Control Activities Project
KIOST	Korea Institute of Ocean Science & Technology
FFA	Pacific Islands Forum Fisheries Agency Secretariat
SPREP	Secretariat of the Pacific Regional Environment Program
AIS	Automatic Identification System
S-AIS	Satellite-based Automatic Identification System
RSP	Regional Surveillance Picture
RFSC	Regional Fisheries Surveillance Centre
MCS	Monitoring Control and Surveillance
VMS	Vessel Monitoring System

1. Project

Project Title	Republic of Korea-Pacific Islands Remote Sensing Surveillance System for Supporting Illegal, Unreported and Unregulated (IUU) Fishing Control Activities Project	
Donors	– Government of Korea – Pacific Island Forum Secretariat (PIFS)	
Implementing Agencies	– Korea Institute of Ocean Science & Technology (KIOST) – Pacific Islands Forum Fisheries Agency (FFA)	
Involved Countries	Cook Islands Federated States of Micronesia Fiji Kiribati Republic of the Marshall Islands Nauru Niue	Palau Papua New Guinea Samoa Solomon Islands Tonga Tuvalu Vanuatu

2. Funding

Payment/Agency	1st Payment	2nd Payment	3rd Payment
KIOST	$310,000	$310,000	$620,000
FFA	$130,000	$130,000	$260,000
Secretariat (Administration Fee)	$60,000	$60,000	$120,000
Total	**$500,000**	**$500,000**	**$1,000,000**

3. Project History

'15. Sep. 14-17 (PIFS-KIOST) First meeting (revising subsidiary arrangement, project management)

(KOR-PIF) Technical meeting at PIFS for arranging project object and contents

'15. Oct. 28 Signed: **Subsidiary Arrangement**

'15. Nov. 3-4 (KIOST) attended "Symposium for Promoting Korean Overseas Fisheries Companies' Corporate Social Responsibility (CSR) towards the Pacific Region" and presented "Satellite Remote Sensing and its Application for Fishery Resource and Coastal management in PIF Region''

(KIOST-MFMRD) Visited Ministry of Fisheries and Marine Resources Development of Kiribati to understand fishery monitoring status of PIF region / Collecting project requirements

'16. Jul. 29-30 (KIOST-FFA) KIOST visited FFA to meeting for arranging project contents and understand FFA status

'16. Sep. 15 Signed: **Revised Implementation Agreement**

'16. Nov. 02 (FFA) Two FFA staff visited KIOST to discuss FFA status and project plan

'17. Mar. 27-28 (KOR-PIF) Critical Design Review

'17. Oct. 26 Signed: **Deed of Amendment** (Change project end date to 19. 12. 31)

'18. Aug. 09-10 (PIF-KIOST) Annual project update meeting & visit Samoa IUU control facilities

'18. Sep. 02-19 (FFA) A FFA staff visited KIOST and MOFA to report project progress

'18. Nov. 26-29 (KOR-PIF) Mid-Term Review & Annual Technical Evaluation & Attending PGRSC

'19. Sep. 23-27 (KIOST-FFA-CSIRO) Technical workshop for checking project progress and discussing future cooperation

'19. Nov. 28-29 (KIOST) KIOST attended "Pacific GIS and Remote Sensing Council (PGRSC) 2019" and presented "Remote Sensing Surveillance System for Supporting Illegal, Unreported and Unregulated (IUU) Fishing Control Activities"

(KIOST-FFA-CSIRO) Discussion on utilization of NovaSAR for future usage

& Future collaborate plan

'19. Dec. 04-14 (FFA) A FFA staff visited KIOST and MOFA to report project progress

'19. Dec. 31 Project End

Figure 1. Meeting at Ministry of Fisheries and Marine Resources Development at Kiribati (Nov. '15)

Figure 2. Meeting at FFA (Jul. '16)

Figure 3. CDR meeting at Nadi, Fiji (Mar. '17)

Figure 4 Annual meeting at Apia, Samoa (Aug. '18)

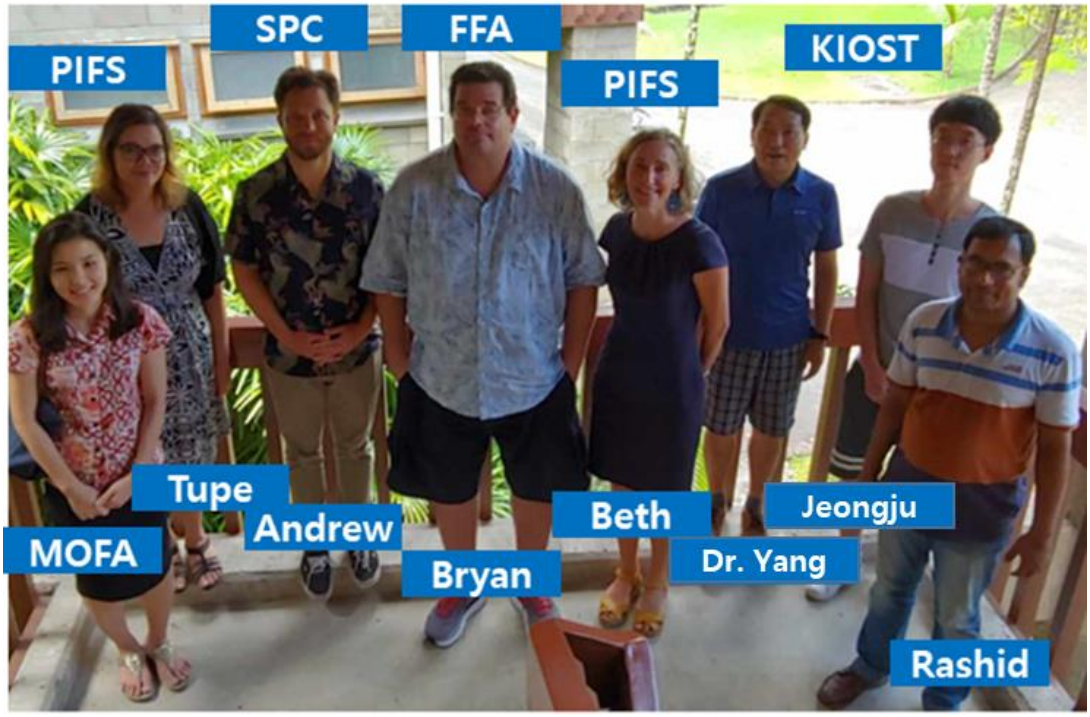

Figure 5. Mid-Term Review (Nov. '18)

Figure 6. Technical meeting at CSIRO (Sep. ‘19)

4. Project Overview

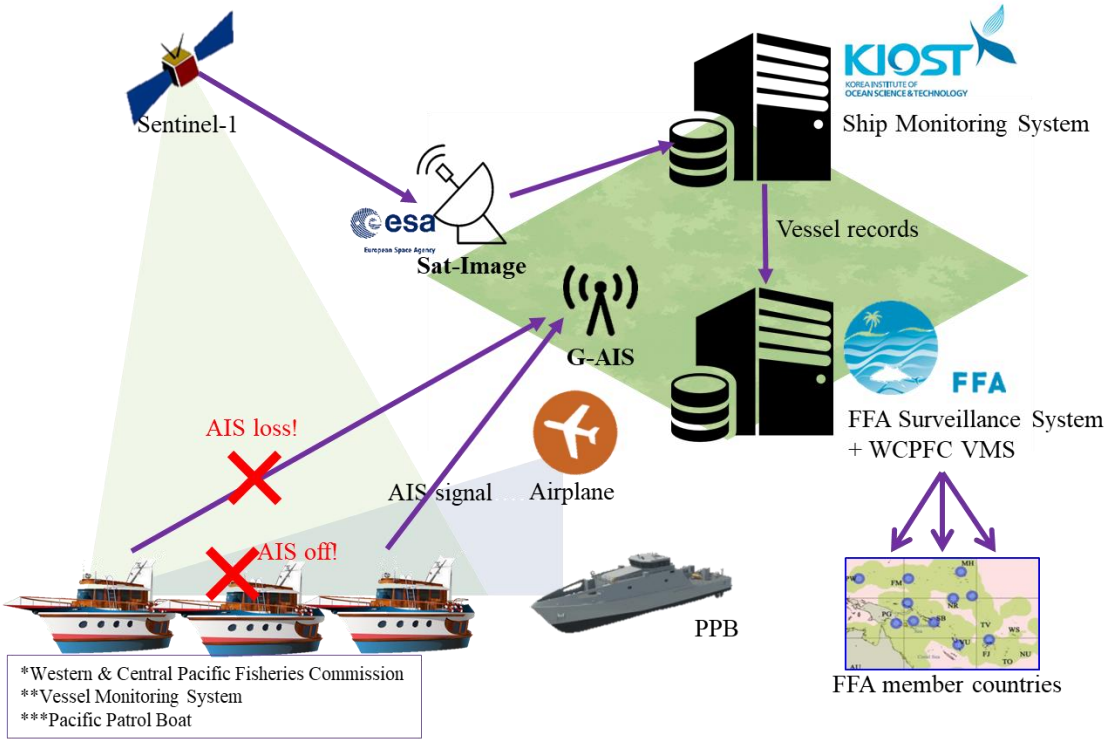

Figure 7. Project Overview

The basic concept of ship detection system is to acquire Sentinel-1 data provided by ESA and detect vessels and share the results to FFA (Figure 7).

Usually, vessels need to report their position through radio communication (e.g., AIS) to the VMS. However, vessels operating illegally have the problem of turning off the AIS (or other machine) transmitter. Also, ships far from the ground station are also difficult to locate due to the loss of position report signals. For this reason, it is necessary to use satellites to monitor vessels that are involuntary for monitoring or in the far ocean.

This project aims to use Sentinel-1 because it is a satellite equipped with SAR sensors for day and night surveillance using microwave can penetrate the cloud. The project output is expected to be support IUU surveillance and control activities with synergetic usage with local surveillance infrastructure such as PPB and airplane.

5. Main Project Outputs and Indicators

5.1 Item 1 – Development Ship Detection Module (KIOST)

In accordance with the project plan, KIOST developed a Sentinel-1 ship detection system during project period. The goal of the system is to download the Sentinel-1 image and then detect and display the detected vessel using proper satellite image processing techniques. To achieve this goal, the ship detection system was developed in following four modules: Sentinel-1 acquisition module, Sentinel-1 pre-processing module, Sentinel-1 ship detection module, and Sentinel-1 visualization module.

To explain the KIOST achievements, in this section, first, overall system diagram (Figure 8) is described and then the function of each submodule is explained.

5.1.1 Sentinel-1 Ship Detection System

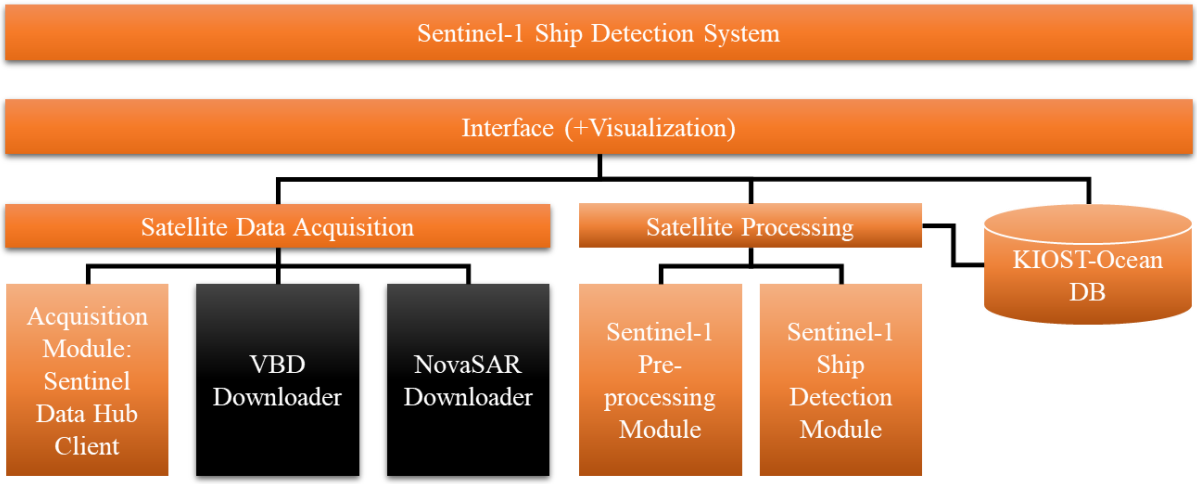

Figure 8. Ship detection system module diagram

Above diagram describes an overview of the KIOST ship detection system. In addition to the Sentinel-1 acquisition, pre-processing and detection module, database and interface were added to complete the operational ship detection system.

The interface part was designed to control each functionality of the ship detection system easily and to handles data request from the outside, likes FFA system. If the FFA system requests ship detection results, this interface then provides ship detection results. Therefore, the visualization module was absorbed in this part.

Plus, PostgresSQL database was adopted to manage and store of vessel data.

5.1.1.1 Sentinel-1 Acquisition Module

Open Search Queries examples

The [query] in the open search URI will follow the same syntax used in the full text search. Here below we provide some examples.

Example	Open Search
Searches every product with SLC product type or products containing the string "SLC" in the metadata	https://scihub.copernicus.eu/dhus/search?q=SLC
Searches every product with SLC product type and S1 sensor Mode or products containing the strings "GRD" and "S1" in the metadata	https://.copernicus.eu/dhus/search?q=GRD AND S1
Search every products ingested in the last day	https://scihub.copernicus.eu /dhus/search?q=ingestiondate:[NOW-1DAY TO NOW]

Figure 9. API example of Copernicus Open Access Hub

ESA provides Sentinel data at free of charge through their website, named 'Copernicus Open Access Hub.' This site provides a search function for Sentinel-1 data, and also Sentinel-2 data is also available through this website, which will be used at future.

Copernicus Open Access Hub provides the Open Search API (Figure 9). This API allows programs to automatically retrieve and download data without the need for human interaction.

Based on this API, KIOST has developed a download module (Figure 10). This is a Windows Winform-based GUI program that includes most of the functionality provided by the Hub. The ESA policy does not limit the number of data downloads, but the number of simultaneous downloads is limited to two. In South Korea, it takes about 10 to 30 minutes to download a single Sentinel-1 data from the Hub.

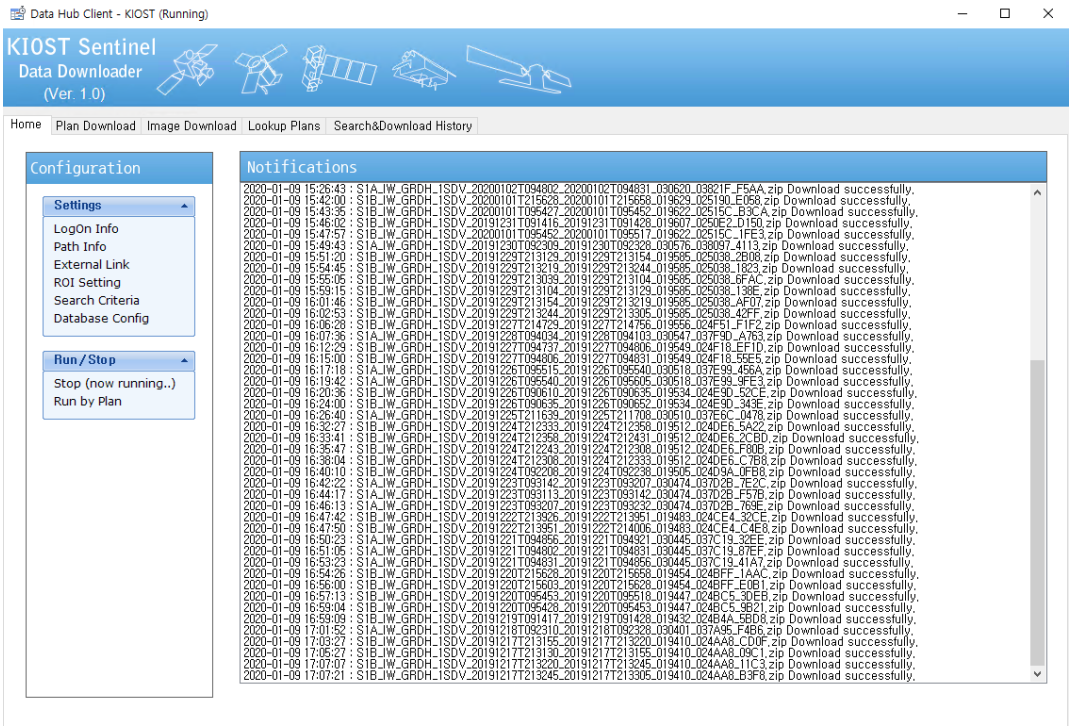

Figure 10 Capture image of Sentinel acquisition module

5.1.1.2 Sentinel-1 Pre-processing Module

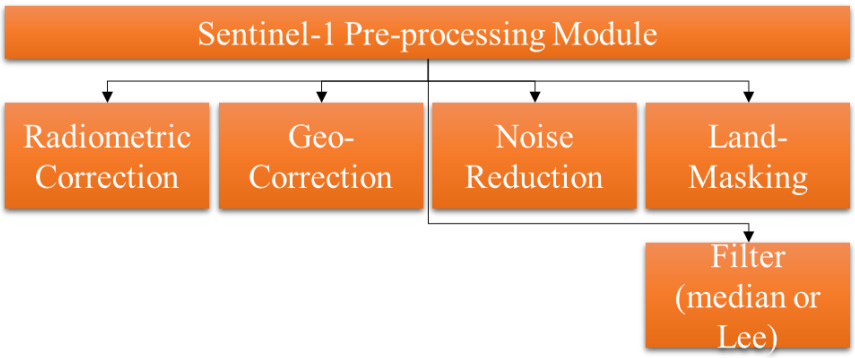

Figure 11. Function of Sentinel-1 pre-processing module

Since the Sentinel-1 data contains distortion like radiometric distortion and geometric distortion, ship detection using original Sentinel-1 data often generates the imprecise results. Therefore, pre-processing processes are required (Figure 11).

Pre-processing is used to each of the following purposes:

- Radiometric Correction: To correct for radiometric distortion caused by atmospheric absorption, scattering and sensor calibration. It is also for converting the value of image data expressed as digital number, not physical quantity, into σ0 ("sigma nought") related to Radar cross section.
- Geometric Correction: To correct SAR image which is affected by the direction of flight and beam direction, and other geometric errors caused by various causes.
- Noise Reduction: To reduce after image of ships due to the phase error of radar system caused by ship's movement and radio frequency interference (RFI) on C-band. Radio interference on C-band in the WCPO area is rare, but afterimages caused by phase error due to ship movement should be eliminated.
- Land-masking: To exclude land, islands and coral reefs that are difficult to distinguish from ships in radar images.
- Filter: To mitigate speckle noise.

The whole pre-processing steps take less than 10 minutes on an i9 processor.

Figure 12 shows the example of pre-processed image.

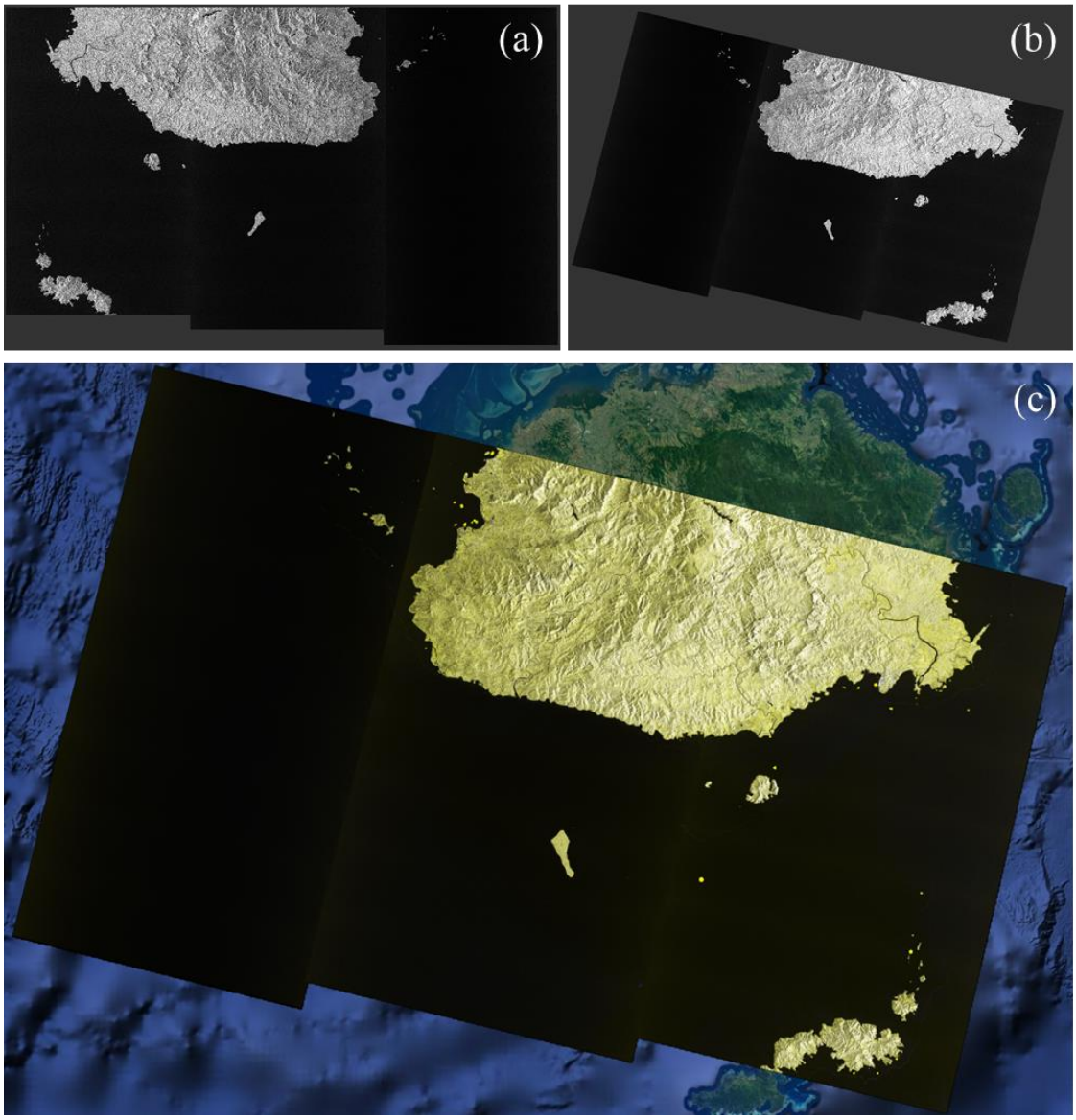

Figure 12. (a) Sentinel-1 GRD image from Fiji (b) Geo-corrected image (c) Google Earth Pseudo-colored image

5.1.1.3 Sentinel-1 Ship Detection Module

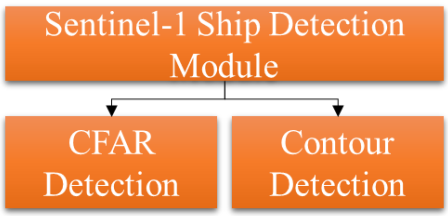

Figure 13. Function of Sentinel-1 ship detection module

Images that have been pre-processed and land-masked, leaving only the ocean, are easy to find ships. Because microwaves are more reflective at the vessel surface than at sea surface, the vessel in the Sentinel-1 SAR image is represented by a bunch of bright pixels.

Sentinel-1 Ship Detection Module has 2 functions: CFAR Detection and Contour Detection (Figure 13).

Moving window CFAR Detector is a method of detecting locally bright pixels, which is advantageous for detecting ships in SAR images.

Contour Detection is a method of detecting boundary (or simply it can be referred as object detection). It detects the boundary values of various objects appearing on a SAR image.

The below two formula describes CFAR detector adopted ship detection system. PFA means probability of false alarm. According to the defined PFA, the value of t in the below equations is determined, and according to the value of t, only pixels brighter t sigma than the surroundings are selected. The result is, only locally bright pixels are selected.

$$PFA = \int_{T}^{inf} f(x)dx = \frac{N(p_{threshold})}{N(P_{total})}$$

$$PFA = \frac{1}{2} - \frac{1}{2} erf\left(\frac{t}{\sqrt{2}}\right)$$

$$Intensity(x) > \mu_{background} + \sigma_b * t$$

After performing CFAR detection, the chunks of bright pixels are extracted into objects through contour detection. Most of these extracted objects are ships.

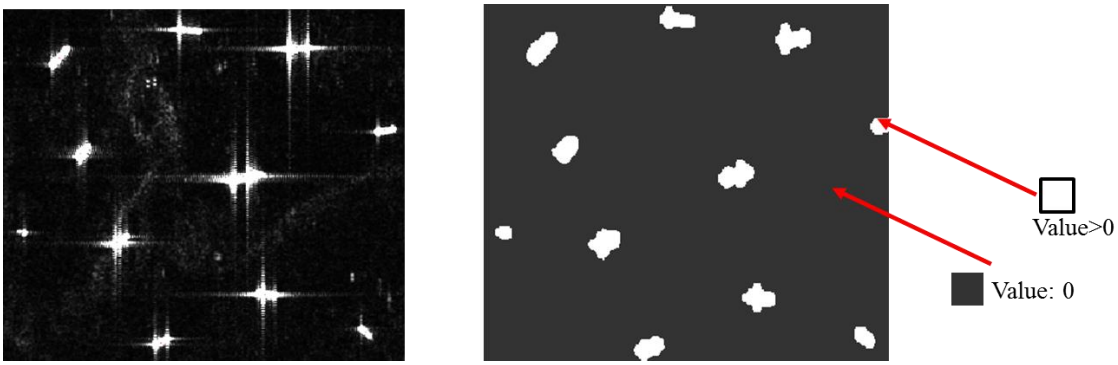

Figure 14. (Left) Sentinel-1 SAR image (Right) CFAR detection applied image

5.1.1.4 Sentinel-1 Visualization Module

12. KIOST moving visualization module for themselves to GoogleEarth (GE), possible additional collaboration

Figure 15. Sentence 12 in Critical design review report

As discussed at the critical design review meeting on March 27, 28, 2017, KIOST decided to use Google Earth for visualization to provide ship detection results. Therefore, KIOST has developed a visualization module to output vessel detection results in the KMZ format used by Google Earth.

Adopting Google Earth has a many advantages. It is free, independent of operating environment, and has many users. It can therefore be used in other oceanic/geometric applications and can easily be integrated in existing FFA monitoring system which is using Google Earth.

Considering the network capacity of WCPO area, the generated ship detection result KMZ file contains 'vessel chipset' extract from Sentinel-1 image, not the entire image of Sentinel-1.

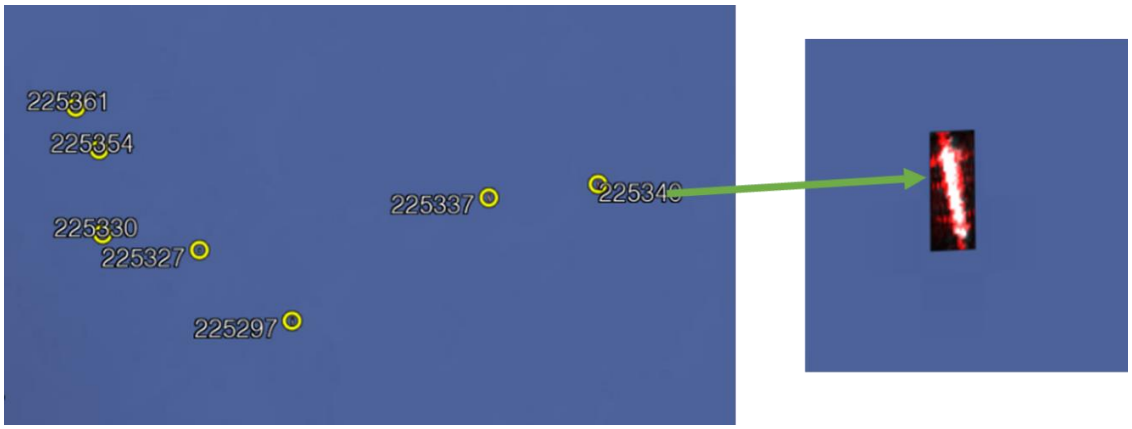

Figure 16. Sentinel-1 Chipset output

By adopting this chipset format, the ship detection result generated from a single Sentinel-1 data shows that the KMZ file is smaller than 3 MB while entire Sentinel-1 image KMZ file is usually larger than 150 MB.

As explained in section 5.1.1, since it will be directly utilized with FFA system, so it is absorbed in the interface part.

Ship monitoring results likes above figure will be provided following HTTP GET request:

http://KIOST/v1/search/query?datatype=sarship&xfrom=**{minLon}**&xto=**{maxLon}**&yfrom=**{minLat}**&yto=**{maxLat}**&datefrom=**{yyyyMMddHHmmss}**&dateto=**{yyyyMMddHHmmss}**&format=**{kmz or json}**&file=**{true or false}**

To get the KMZ results of the Sentinel-1 detection on December 11, 2019 for Fiji's waters, following GET request will work.

http://KIOST/v1/search/query?datatype=sarship&xfrom=175&xto=180&yfrom=-20&yto=-15&datefrom=20191205000000&dateto=20191206000000&format=kmz

Ship detection result is also provided in json format for easy handling. After FFA opens REST API to collect json result, the ship detection system can automatically send via POST API.

5.1.2 Land-Masking Dataset

As described in 5.1.1.3, the ship detection system uses a moving window CFAR detector to extract locally bright pixels from the Sentinel-1 imagery. Therefore, the pixels in the land cause incorrect results in CFAR detector due to the high intensity. To prevent it, land-masking is performed, and it requires land dataset.

The General Bathymetric Chart of the Oceans (GEBCO) is often used for this purpose, however the resolution is low and not proper to use to coastal area.

Therefore, KIOST made new land-masking dataset using AW3D30 provided by The Japan Aerospace Exploration Agency (JAXA). AW3D is a digital surface model which has height above sea level in meter in land area and NaN for ocean area. This data, freely available in 30 m resolution, has a significant advantage over GEBCO for land-masking purposes. Since JAXA updates AW3D30 periodically, it is better than Shuttle Radar Topography Mission (SRTM) data which published late 2014 which is widely used such as Sentinel Application Platform (SNAP).

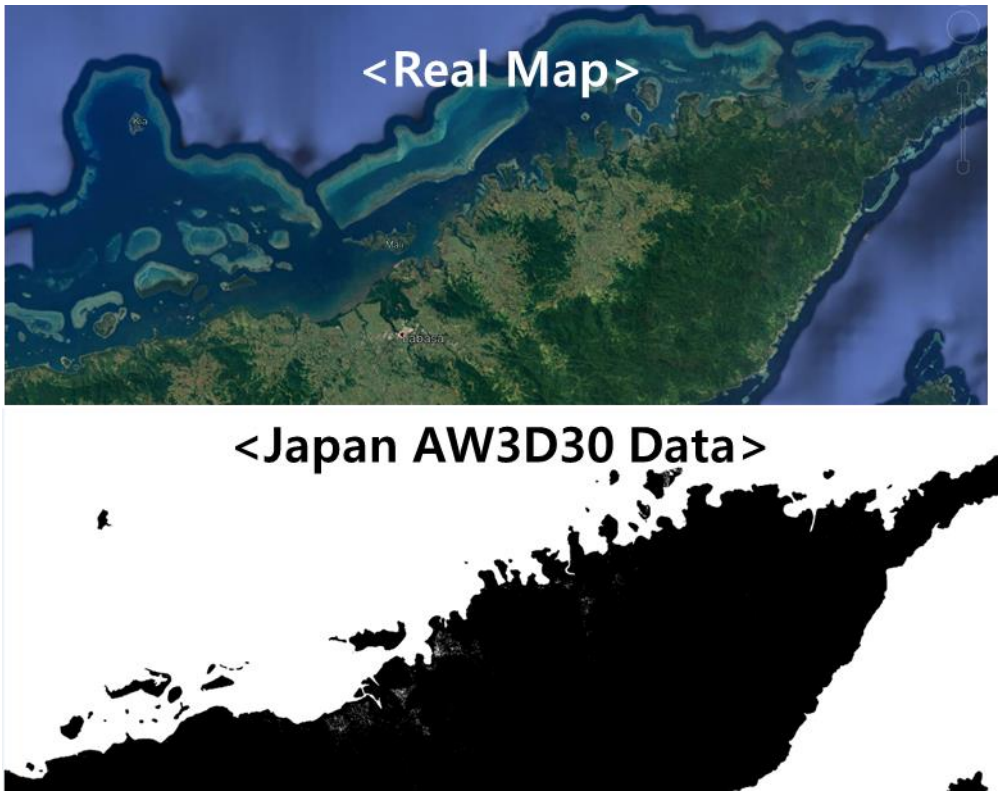

Figure 17. Comparison of Google map and AW3D30 images: (Top) Google Earth and (Bottom) AW3D30 comparison in the Northern Division region of Fiji

However, there are a lot of small islands is omitted and since it is surface model, it does not include atoll, reef barriers, and etc. To handle this issue, KIOST is additionally used Landsat-8 for some areas like Fiji and Samoa (Figure 18). In addition, AW3D30 was converted to bit (0 and 1) data because only the distinction between land and ocean is needed (Figure 17).

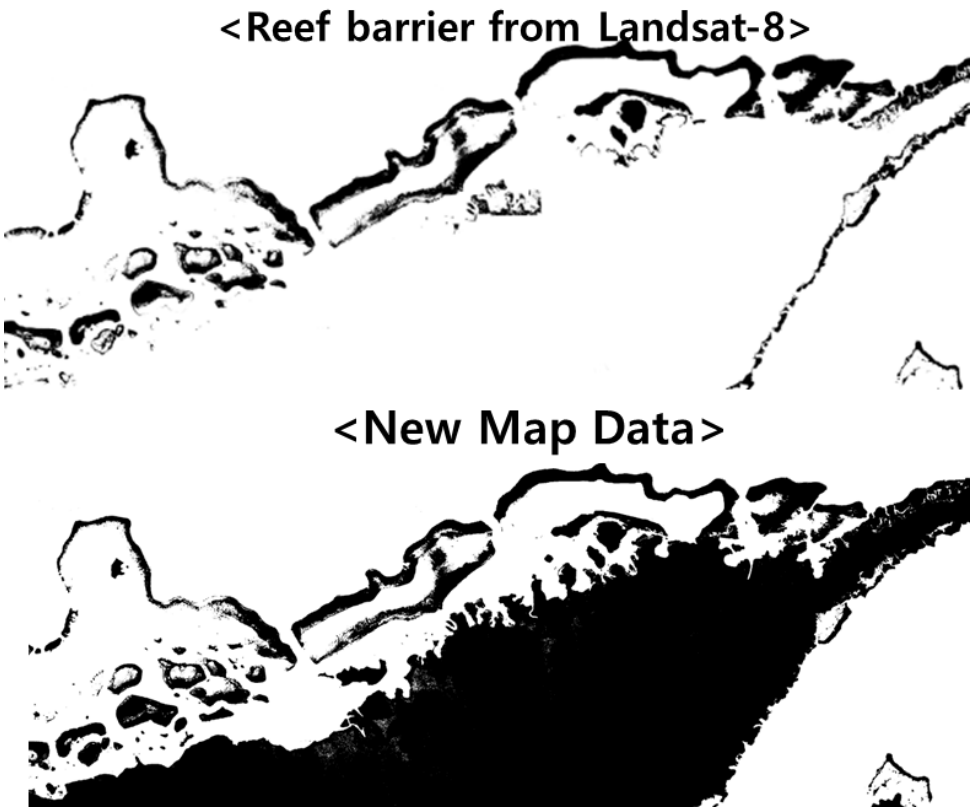

Figure 18. Comparison of Landsat-8 and AW3D30: (Top) Extracted additional object from Landsat-8 (Bottom) New land map data using AW3D30 + above image

5.1.3 Ship Detection Result

During the early December 2019 FFA staff visited KIOST, a review of ship detection result for area around Fiji and Samoa was conducted. For the reviewing the ship detection result in Fiji, Sentinel-1 imagery which was taken at 17:40 on December 5, 2019, UTC. For the Samoa, 06:00 December 11, 2019 UTC image was used.

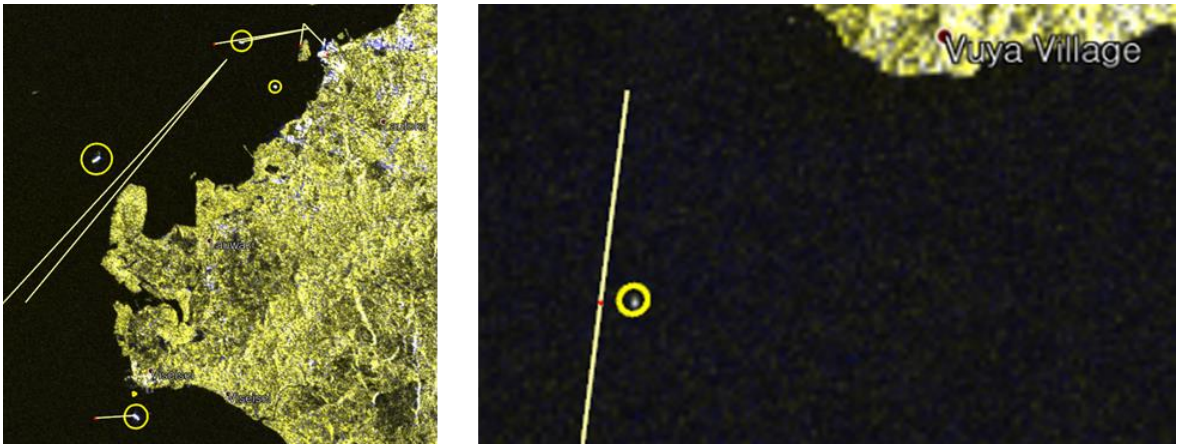

Figure 19. Yellow Circle: Sentinel-1 ship detection result, Yellow line: AIS trace provided by FFA: (Left) Result on Western Division of Fiji (Right) Passenger ship between the Central and Northern Divisions

Due to the phenomenon called azimuth shift in SAR imagery, moving vessels are found slightly off the actual position. Although location of AIS trace and SAR image is little bit different, actually it is matched. The main cause of azimuth shift is well-known therefore KIOST will improve this coordinate error.

Since the resolution of Sentinel-1 is 20 m, ship detection result was shown that ships which size is less than 40 m were seldom detected. KIOST is aware of this issue and therefore is working on detection techniques not only CFAR detection to make the better ship detection result.

Figure 20. Unidentified object suspected as a ship

Despite of the weakness described above, the objective finding vessels not identified by AIS or the like could be achieved.

Figure 21. Ship detection result (Samoa)

For the Samoa region, only one vessel marked '224224' was detected and confirmed to be consistent with the VMS data of the FFA.

In addition, KIOST is conducting detailed verification using AIS data around Korean Peninsula which is collected KIOST-self.

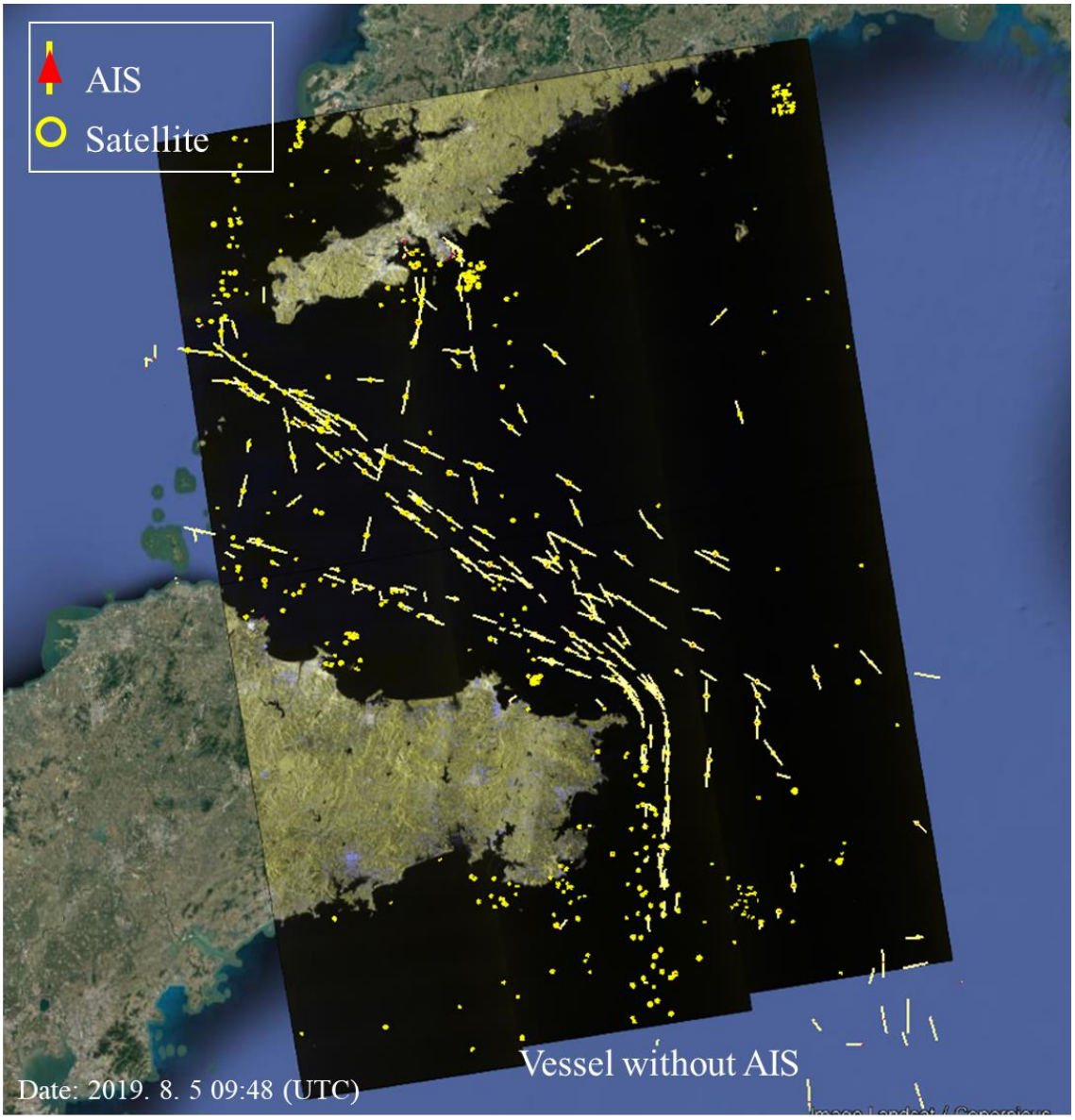

Figure 22. Ship detection result from Yellow Sea

The results of vessel detection using Sentinel-1 data obtained from the Yellow Sea on August 5, 2019 are as follows

- A) Number of AIS vessels: 267
- B) Number of SAR detected ship matched with AIS: 235 (88%)
- C) Number of AIS vessels not matched Sentinel-1 result: 32 (12%)
- D) AIS existed but not visible in the SAR image: 28 of 32 (C)
- E) AIS existed also visible in the SAR image, but not detected: 4 of 32 (C)
- F) Number of missing vessels by land-masking because it is close to land: 3 of 4 (E)

Total ratio of SAR-AIS matching: 88%

Processing time: < 15min @ i9

5.1.4 Academic Activities About Ship Detection

Conference presentation

2016. 10. 13, Development of SAR Image Enhancement Method for Automatic Ship Detection, Fall conference of the Korean association of geographic information studies/ Jeongju Bae, Chan-Su Yang

2016. 11. 24, A Study of Reduction Landmasking Error on SAR Image for Automatic Ship Detection, Fall onference of the Korean society of marine environment & safety/ Jeongju Bae, Chan-Su Yang

2017. 5. 17, GPU-based Parallel Computing for Processing Sentinel-1 SAR Image, International Symposium on Remote Sensing 2017/ Jeongju Bae, Chan-Su Yang

2017. 5. 17, An improved method of land masking for KOMPSAT-5 images using Sobel edge detection and electronic navigation chart, International Symposium on Remote Sensing 2017/ Ju-Han Park, Harun-al Rashid Ahmed, Chan-Su Yang

2017. 10. 13, Monitoring of Coastal Structure & Topography Changes Using Satellite-based Synthetic Aperture Radar Imagery, Fall conference of Korean Society of Coastal Disaster Prevention/ Ju-Han Park, Chan-Su Yang

2018. 11. 9, Maritime Domain Awareness (MDA): Ship Detection and Classification by Spaceborne Synthetic Aperture Radar, ICSANE 2018/ Kazuo Ouchi, Gerard M. Martin, Chan-Su Yang

2019. 7. 29, SATELLITE IMAGE-BASED SHIP CLASSIFICATION METHOD WITH SENTINEL-1 IW MODE DATA, IEEE International Geoscience and Remote Sensing Symposium 2019/ Seungryong Kim, Jeongju Bae, Chan-Su Yang

2019. 8. 9, REMOVAL OF DIFFERENT TYPES OF NOISES IN SYNTHETIC APERTURE RADAR (SAR) IMAGES FOR IMPROVED SHIP DETECTION, IEEE International Geoscience and Remote Sensing Symposium 2019/ Ju-Han Park, Chan-Su Yang, Harun-al Rashid Ahmed, Kazuo Ouchi

2019. 10. 31, Estimation of Ship Velocity from Multispectral Satellite Image, ICSANE 2019/ Tae-Ho Kim, Jeongju Bae, Chan-Su Yang

2019. 10. 31, Performance Evaluation of Ship Detection Using Sentinel-1 IW Data, ICSANE 2019/ Seungryong Kim, Chan-Su Yang

2019. 10. 31, Practical Approach for Noise Reduction in Synthetic Aperture Radar (SAR) Images, ICSANE 2019/ Ju-Han Park, Chan-Su Yang

Paper

2018. 3. 26, An Improved Method of Land Masking for Synthetic Aperture Radar-based Ship Detection, The Journal of Navigation / Chan-Su Yang, Ju-Han Park, Harun-Al Rashid, (SCIE)

2017. 8. 31, Land Masking Methods of Sentinel-1 SAR Imagery for Ship Detection Considering Coastline Changes and Noise, Korean Journal of Remote Sensing/ Jeongju Bae, Chan-Su Yang (Korea Citation Index)

5.2 Item 2 – Background Study for Preparing Project 2nd Phase (KIOST)

To propose and prepare the project second phase, KIOST conducted studies about other satellites. Additional satellites studied for monitoring WCPO area to use 2nd phase as follows: Sentinel-2, Radarsat, NovaSAR, NPP VIIRS (VBD product.)

Radarsat and NovaSAR are SAR satellites that provide data similar to Sentinel-1. Instead of studying them, KIOST is conducting a proof-of-concept (POC) study on the VBD products of NPP VIIRS and Sentinel-2, which are not SAR satellite but multispectral (optical) satellites.

An example of the result of a study on ship detection using Sentinel-2 is shown below.

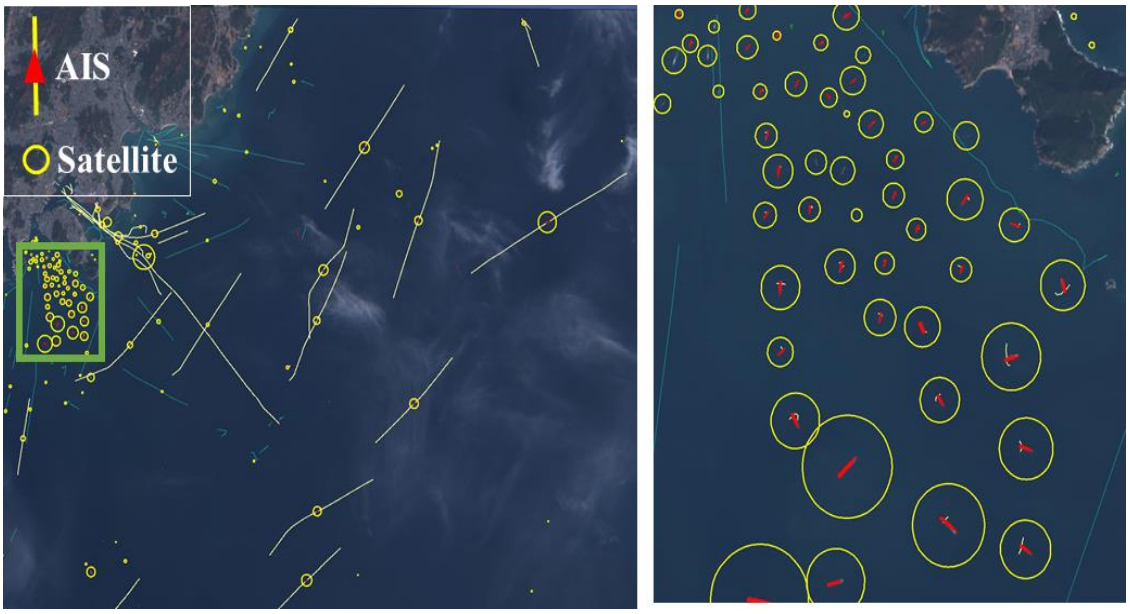

Figure 23. Sentinel-2 ship detection result (test purpose)

The result is generated automatically by the ship detection system, and it is expected that Sentinel-2 is also useful to monitor ships if cloud is handled properly (because cloud is white and bright, so they can be confused with ships or ship wakes by ship detection system.)

If proper pre-processing algorithm which considers optical characteristics is developed, it will be helpful in monitoring IUU fishing in the WCPO region.

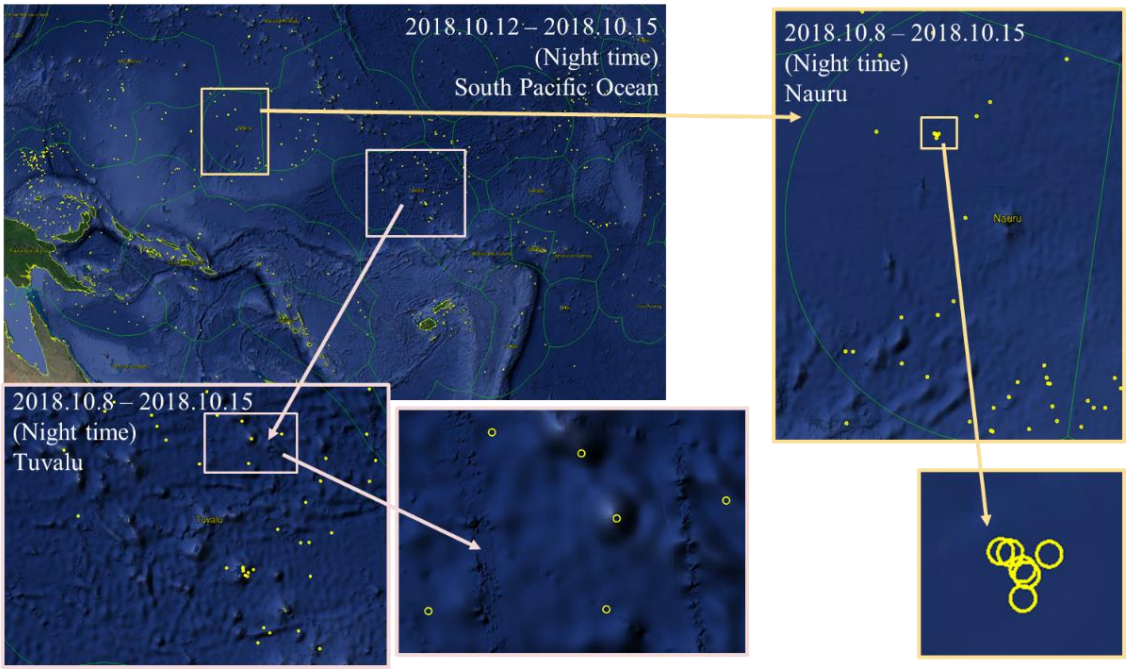

Figure 24. NPP VIIRS VBD product on WCPO region

KIOST also conducted a study of the NPP VIIRS VBD product. This data is obtained at night, and contains the fishing boats which lighting up and operating at night. Since the data are obtained 1-2times a day for extensively wide area, it will be useful for monitoring night fishing vessels.

5.3 Item 3 – Project Promotion (KIOST)

KIOST is working on making video like Figure 25 and brochure likes Figure 26 for promotion.

Figure 25. Title scene of promotion video

Figure 26. Cover page of promotion brochure

5.4 FFA's role in the project had multiple aspects. These include:

- Developing a process for dealing with and storing received remote sensing detections;
- Technical delivery of processed and analysed detections to members for integration into existing workflows;
- Capacity development of both FFA Secretariat staff and Members on the engagement of SAR for fisheries enforcement; and
- Engagement with FFA members.

FFA came to this project with very little capacity or understanding of remote sensing utilisation in fisheries enforcement. A significant investment of staff time was required to up skill FFA staff, which occurred throughout the project.

FFA focused on integrating remote sensing data and displaying it in existing Regional Fisheries Surveillance Centre (RFSC) system. After implementing an initial system of just recording and displaying the reported contacts, it became apparent that the sensed area boundary was important for understanding in the analysis. Eventually this process was adapted and has become the standard technical display for analysis of contacts from all sources in the RFSC. The analyst assigns a "compliance index" to the reported contact detection. The final portion of the technical solution involved linking with KIOST for an automatic secure transfer of detection data using mechanisms based on an industry standard of REST API.

For reported SAR contact detections, the compliance rating adopted was essentially binary scale, 0 if a matching vessel was reported on any other system (ie AIS or VMS), or -5 if not able to be correlated.

FFA Secretariat engagement with members on remote sensing was focused on attachments during the four annual regional MCS operations. This capability and engagement developed over the period of the project culminating in the project sponsoring two FFA member participants into the analysis cell of the RFSC during Operation Kurukuru 2019. In addition, briefings to the FFA membership on the project was also conducted at the annual MCS Working Group meeting.

As FFA's understanding of the capabilities of remote sensed data improved, the envisioned role within the MCS process was adjusted. For example we learned that analyst's using the developed analysis process it is relatively easy to cross match remote sending data with existing VMS or AIS reported positions. However, the information reported by the SAR was insufficient to identify vessel, so for MCS purposes it was important to have a response enforcement asset to cover scanned areas to further verify vessels. After several trials using the patrol boats as the response asset, this was discontinued, mainly because the large area covered by SAR could not be adequately scanned by the response enforcement asset. Subsequent trials using surveillance aircraft commenced and while several encouraging trials have been conducted they are still being shaken out. Operationally the utilisation of SAR with surveillance aircraft is looking to be of operational benefit. The exact method operation is still to be determined.

In a case of fortunate timing for the FFA secretariat, two FFA members independently engaged in remote sensing trials during the period of the project and the secretariat was able to provide assistance because of the capacity developed through this project.

A small but final point is that FFA co-contributed to this project with staff time and resources to the project.

6. Project Beneficiaries

The project directly benefits 14 Pacific Island Countries' Fisheries and Maritime Enforcement Agencies. These countries are Fiji, Nauru, Tonga, Republic of the Marshall Islands, Tuvalu, Samoa, Niue, Vanuatu, Papua New Guinea, Solomon Islands, Kiribati, Palau, Federated States of Micronesia, and Cook Islands.

7. Toward a Project Second Phase

This project has shown the potential for remote sensing to be integrated into the Monitoring, Control and Surveillance (MCS) efforts in the Western and Central Pacific Ocean (WCPO) by the Pacific Islands countries (PIC). However much remains to be explored to ensure the long term application of remote sensing

- Standard Operating Procedures for the use of remote sensing
- Exploration of non SAR data sources in the region

7.1 Previous result

As a result of the previous project, named 'Remote Sensing Surveillance System for Supporting Illegal, Unreported and Unregulated(IUU) Fishing Control Activities', KIOST tested the ship detection in the Pacific region using Sentinel-1 satellite. Additionally, the verification using AIS of Korean water, which KIOST collected, showed a 88% Sentinel-1 and AIS matching ratio

- In addition to the ship detection based Sentinel-1 SAR data, high resolution map data of the Pacific region was made which applicable for all satellite based application. It can be used to monitor the Pacific region using various satellites, e.g., Sentinel-2, ICEYE
- Through the previous project, FFA now has experience and capacity of satellite application.
- There is arising potential to use deep learning and big data technologies due to the its' maturity.
- Based on these backgrounds, there is a possibility of introducing additional multiple satellites equipped with various sensors and state-of-the-art technologies on IUU surveillance systems.
- There is a necessity of utilization research on multi-spectral optical satellite such as Sentinel-2 and PlanetScope for day-time monitoring, and NPP VIIRS for night-time monitoring.

Figure 27. (Left) Fishing boat in night operation (Right) Night fishing boat seen in the image.

7.2 Second phase plan

7.2.1 KIOST

● Development of fishing vessel monitoring system using satellite data as follows:

1) Application Research for a specified area
- Synthetic Aperture Radar (SAR) except Sentinel-1(ex. Radarsat, NovaSAR)

2) Daytime optical (multi-spectral) sensor data: Sentinel-2(10-20m resolution)
- Nighttime visible/infrared imaging radiometer data: Daily operational purpose

● Development of ship classification algorithm using neural network, statistics, and bigdata

7.2.2 FFA

1) Operational usage of multiple satellites (SAR, optical, VIIRS)/Capacity building
2) Combined utilization of satellite & local surveillance (patrol boat, aircraft, etc):Satellite application and feedback to improve the system

7.2.3 PIFS

1) Managemnet & Evaluation of the project

7.3. Project goal

1) Shor term goal
- Development and opration of IUU surveillance system using multiple satellites
- Capacity building for multiple sensory satellites of PIF nations

2) Long term goal
- Supporting the Pacific region to monitor IUU fishing activities using multiple satllites for sustainable fishery and environment preservation
- Cooperative research of KOR-PIF

8. Financial Report

8.1 The financial acquittal report for KIOST is detailed below.

Category	Line Item	Amount (USD)
Carry Forward of Funds	Second half of 2019 Budget	**520,376.34**
Research Cost	Payroll cost Research activity (including travel expenses) Expenses for research material	(171,475.81) (100,658.73) (248,241.80)
Total expense		(518,876.34)
Balance of funds for the project at 31 December 2019		Approx. 1,500

8.2 The financial acquittal report for FFA is detailed below.

Category	Line Item	Amount (USD)
Carry Forward of Funds	Second half of 2019 Budget	72,541.00
Attachment/Trainee Support	1 Cook Island attachment (Solomon Islander attachment at no cost as in country)	(5,021.45)
Travel Support	Technical exchanges with KIOST	(15,197.55)
Imagery Acquisition	Additional Remote Sensing Processed Acquit ions	(49,041.87)
Equipment	Office Equipment for project	(4,855.33)
Total expenses		(74,116.20)
FFA Fund adjustment		1,575.20
Balance of funds for the project at 31 December 2019		-

9. Acknowledgement

The project would like to acknowledge the support and collaboration of the following organizations:

- The Pacific Islands Forum Secretariat (PIFS)
- The Korean Ministry of Foreign Affairs (MOFA)

We also acknowledge the European Space Agency (ESA) for the providing high-quality SAR product.

10. Main Contacts

KIOST:
Dr. Chan-Su Yang
Principle Research Scientist
Marine Safety Research Center
Tel No: +82-51-664-3615
Email: yangcs@kiost.ac.kr

FFA:
Allan Rahari
Director Fisheries Operations
Pacific Islands Forum Fisheries Agency
Tel No: +677 21124
Email: allan.rahari@ffa.int

Annex1. Published Papers

THE JOURNAL OF NAVIGATION (2018), **71**, 788–804. © The Royal Institute of Navigation 2018
doi:10.1017/S037346331800005X

An Improved Method of Land Masking for Synthetic Aperture Radar-based Ship Detection

Chan-Su Yang[1,2,3], Ju-Han Park[1] and Ahmed Harun-Al Rashid[1,2]

[1](*Marine Safety Research Center, Korea Institute of Ocean Science & Technology, Busan, South Korea*)
[2](*Integrated Ocean Sciences, University of Science & Technology, Daejeon, South Korea*)
[3](*Korea Maritime and Ocean University, Busan, South Korea*)
(E-mail: yangcs@kiost.ac.kr)

Land masking of Synthetic Aperture Radar (SAR) images is generally accomplished by applying either archived shoreline databases or image segmentation. However, those methods cannot be solely applied to geographical areas complicated with many small islands and exposed rocks. Therefore, we have proposed a new procedure where Sobel edge extraction is applied to detect the edges of all objects from KOMPSAT-5 X-band SAR images, followed by a merging process with the edges from the land objects based on Electronic Navigational Chart (ENC) coastlines. Using the land mask data, geometrically corrected SAR images were masked before applying a ship detection algorithm. This land masking procedure was applied to several images covering different areas of the Korean Peninsula. The results show that land targets such as newly constructed and natural objects were also masked, and thus did not create false alarms during ship detection. Therefore, this method can be used to assist precise ship detection using SAR images in coastal waters.

KEYWORDS

1. Land masking. 2. SAR. 3. KOMPSAT-5. 4. ENC.

Submitted: 18 March 2017. Accepted: 13 January 2018. First published online: 26 March 2018.

1. INTRODUCTION. Image thresholding and morphological analysis of objects are common methods of ship detection from Synthetic Aperture Radar (SAR) data (Chaturvedi et al., 2012). In SAR images, land has higher reflectance values than open sea. Therefore, land masking is an essential step before applying ship detection algorithms to SAR images (Greidanus et al., 2004; Keramitsoglou et al., 2006; Margarit, 2009; Montuori et al., 2010; Pelizzari, 2011). One of the major concerns in SAR-based ship detection is edge extraction. This is critical in images of complicated geographical areas such as the coastal regions of South Korea which possesses many small islands and exposed rocks, complicated by a large tidal range (Jeong et al., 2013). During land masking, small land objects should be

properly masked out in order to reduce the numbers of false alarms during ship detection (Brusch et al., 2011). Moreover, accurate land maps are also useful in assisting detection of sea surface slicks, wind and wave fields, coastal erosion, development of new structures along the coastline, and other features from high-resolution SAR images (Biamino et al., 2015; Jiang et al., 1999; Kim et al., 2014).

Coastline detection algorithms are generally operated in two modes, "shape" and "image" (Margarit et al., 2009). In the shape method, land masking is achieved by superimposing an archived coastline available in the form of shape files (collections of latitude and longitude pairs) (Margarit et al., 2009). The accuracy increases with the increase in number of points used. Some freely available shoreline files are found at several resolutions, including 90 m resolution (Slater et al., 2006). One of the most commonly utilised shoreline databases is called the Global Self-consistent, Hierarchical, High-resolution Shoreline (GSHHS) which possess a good resolution shoreline data set (Brusch et al., 2011; Wessel and Smith, 1996). Another public domain land-water mask is the Shuttle Radar Topography Mission (SRTM) Water Body Data (SWBD) produced by exploiting data acquired during the National Aeronautics and Space Administration's (NASA's) space shuttle radar topography mission (Biamino et al., 2015; Karvonen, 2015; Wessel and Smith, 1996). However, compared to these coastline maps, Electronic Navigational Chart (ENC)-based coastline data is of much higher resolution.

The image approach exploits image analysis techniques (for example, segmentation and edge detection) in order to isolate the coastline for building a mask by discriminating land pixels from sea pixels (Margarit et al., 2009; Romeiser et al., 2005). Image segmentation is the process of partitioning a digital image into several regions of similar features (Al-amri et al., 2010; Ramadevi et al., 2010; Senthilkumaran and Rajesh, 2009), and edge detection is one of the segmentation processes commonly used for digital images (Kodors and Zarembo, 2013). Many techniques for segmentation are in use: interferometry on SAR image pairs (Dellepiane et al., 2004), wavelet-based active contour model (Della Rocca et al., 2004), morphological filtering (Shu et al., 2010), non-local fuzzy C-means algorithm (Feng et al., 2013), mathematical morphology (Mashaly et al., 2014), etc.

Each of these approaches has advantages as well as some limitations. For instance, despite the high quality of freely available coastline databases, they cannot be directly applied to satellite images as the images have often been georeferenced using only the coordinates of the four image corners without ground control points (Biamino et al., 2015; Greidanus et al., 2004; Trivero et al., 2016). Therefore, the geo-positioning of the satellite images has limited accuracy and results in image shifts in the azimuth direction, and a consequent displacement of the land mask resulting in shifting of shorelines from the actual coastline and associated false alarms near the coast (Biamino et al., 2015; Greidanus et al., 2004; Trivero et al., 2016). On the other hand, commonly available land masks usually have accuracy limitations with small islands, intertidal areas and coastal man-made constructions leading to false alarms (Greidanus et al., 2004). To compensate for these limitations, some methods exclude a safety zone near the coast, but that also leads to potential misdetections (Greidanus et al., 2004). Moreover, these methods cannot easily solve the issue of masking very small islands, exposed rocks and sea stacks. Therefore, in detection of small objects such as ships from SAR images, accurate discrimination and masking of land for those regions possessing many small islands and intertidal zone remains to be solved (Yang and Ouchi, 2008). Considering these issues we have applied a combination of both methods. The inaccuracies in image mode operation were avoided by supporting

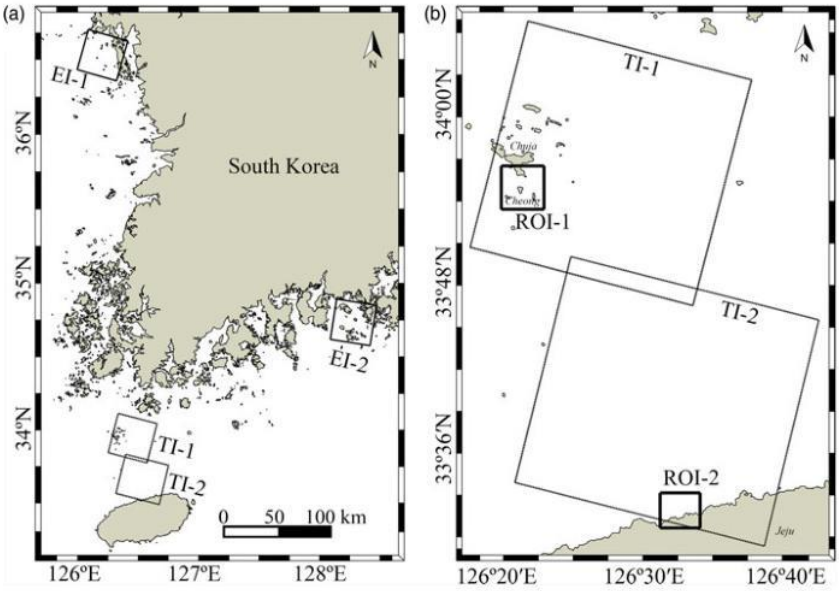

Figure 1. Research area for applying the proposed land masking to KOMPSAT-5 SAR images (the boxes in (a)). Two SAR images (TI-1 and TI-2) were used for the land masking algorithm development, and two images (EI-1 and EI-2) for the method evaluation. ROI-1 and ROI-2 in (b) represent the regions of interest used for the algorithm validation.

image processing with reference shape files. The proposed algorithm takes a temporary land mask image (produced from KOMPSAT-5 images) as input and finalises the land objects from the temporary land mask with the help of a decision-based archived shoreline.

2. MATERIALS AND METHODS.

2.1. *Study area and selected KOMPSAT-5 images.* The proposed method of land masking was first applied to two KOMPSAT-5 images of two different coastal areas in the southern portion of the Korean Peninsula which possess many small islands and exposed rocks (TI-1 and TI-2 in Figure 1). Later on, to check whether this procedure could be used as a general method of land masking in the coastal waters of South Korea, the method was applied to some other images of different regions from which only two images (EI-1 and EI-2 in Figure 1(a)) of complicated regions (geographically complicated due to possessing many small islands) are shown here. The TI-1, TI-2, EI-1 and EI-2 images were acquired on 19 May 2016 10:03:56 UTC, 20 May 2016 10:00:33 UTC, 11 July 2016 10:13:08 UTC, and 22 September 2016 09:15:31 UTC, respectively. TI-1 includes mainly Chuja Island, Cheong Island and some exposed rocks (Figure 2(a)), and TI-2 includes some northern portions of Jeju Island (Figure 2(b)). To show the changes occurring in several steps of the proposed method as well as for comparison with other land masking methods, smaller areas from TI-1 and TI-2 images are considered as regions of interest (ROI-1 and ROI-2, respectively in Figure 1(b) as bordered by small rectangles).

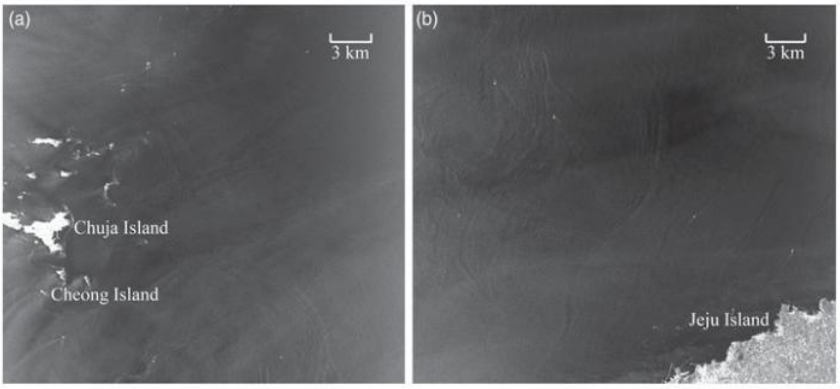

Figure 2. KOMPSAT-5 HH-polarised intensity images: TI-1 (a) and TI-2 (b) (refer to Figure 1 and Table 1).

Table 1. Properties of the KOMPSAT-5 images used in this study.

Properties	KOMPSAT-5			
	TI-1	TI-2	EI-1	EI-2
Acquisition station	KARI	KARI	KARI	KARI
Acquisition date	19 May 2016	20 May 2016	11 July 2016	22 September 2016
Acquisition mode	Standard	Standard	Standard	Standard
Polarization	HH	HH	HH	HH
GSD (m)	2.14	2.15	2.15	2.15
Orbit direction	Descending	Descending	Descending	Descending
Look direction	Left	Left	Left	Right
Incidence angle (°)	36.51∼38.80	31.40∼34.21	45.47∼47.30	47.08∼48.82

KOMPSAT-5 is operated by Korea Aerospace Research Institute (KARI). It is the first South Korean satellite which is capable of acquiring X-band (9.66 GHz) SAR Interferometry (InSAR) at a spatial resolution of up to 1 m (Lee, 2010). It provides all-weather, day and night SAR images for various purposes including ocean monitoring of the Korean Peninsula (Krebs, 2017). KOMPSAT-5 is operated in dual polarisation modes with 10° to 45° incidence angles, and is at an altitude of 550 km (Krebs, 2017). It is capable of collecting imagery in three different modes, namely High Resolution, Standard and Wide Swath Modes (SI Imaging Services, 2015).

The images used in this study are of Level 1A in Standard Mode, which is considered to be the most common imaging mode. Data at this level is already radiometrically corrected and thus requires only geocorrection (SI Imaging Services, 2015). The main imaging characteristics of this mode are Ground Sample Distance (GSD) less than or equal to 3 m with a minimum swath of 30 km (SI Imaging Services, 2015). The properties of the TI-1 and TI-2 images are azimuth angle −90°, wavelength 0.031034 m, frequency 9.66 GHz, altitude around 557 km and azimuth beam width 0.3512°. Some other important properties of the images used in this study are shown in Table 1.

2.2. *Edge detection and land masking.* An edge of an object is an image in a region where changes in image intensity are significant (Kodors and Zarembo, 2013; Singh and

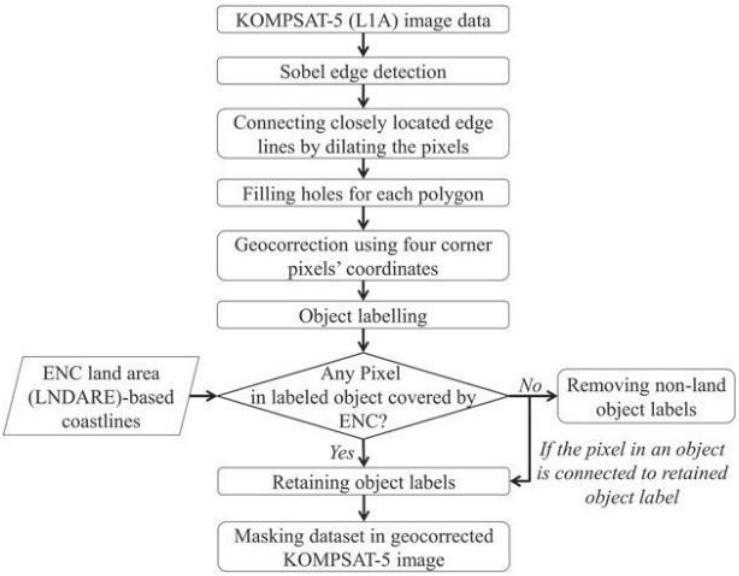

Figure 3. Flowchart of major steps in the proposed land masking.

Kaur, 2013). Thus, an edge can be defined as a set of connected pixels that lie on a particular boundary between two regions (Singh and Kaur, 2013). Edges are used to define the ability to measure the transitions in a meaningful way by preserving useful structural information about object boundaries (Canny, 1986; Simpson, 1990; Singh and Kaur, 2013). When edge points are located, complete boundaries can be formed by linking the points (Singh and Kaur, 2013). Detection of object edges usually consists of three steps: i) filtering to reduce image speckle noise; ii) enhancement to detect changes of intensity in the neighbourhood of a point (pixel) where the gradient magnitudes are computed to indicate the changes of intensity; and, iii) detection to group all elements into two sets of black and white pixels often followed by thresholding (Ramadevi et al., 2010; Senthilkumaran and Rajesh, 2009). The key steps during the proposed land masking of KOMPSAT-5 images are shown in a flowchart (Figure 3). A detailed description of each step follows.

2.2.1. *Object Boundary Extraction.* To extract the boundaries of all objects both the Sobel (Gao et al., 2010; Zhang et al., 2009) and Canny (Canny, 1986; Wall et al., 2008) edge detection filters were separately applied to the images for comparison. The Sobel filter detects strong edges in the horizontal and vertical directions, and all the edges are extracted using a threshold value (Shahane et al., 2015; Sobel, 1990). If high threshold values are applied, signals from very small islands or exposed rocks would also disappear along with the signals from ships. Therefore, suitable threshold values were determined manually (Liu and Jezek, 2004) after applying a set of threshold values starting from 0 and gradually increasing by 0.05 intervals until the edges of all objects were obtained. In this study, a threshold value of 3 was found to produce the best results for all images. The produced images were of binary types where the object edges were generated as thin broken lines. However, many lines were also generated inside the objects during this edge extraction

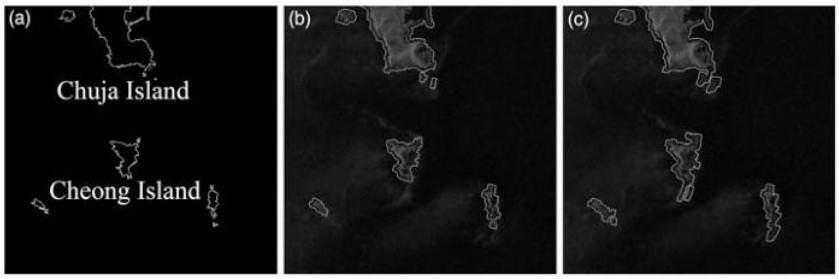

Figure 4. Land boundary detection results for ROI-1 (Figure 1) by ENC-based coastline map (a), proposed Sobel-ENC-based land masking (b), and Canny-ENC-based land masking (c).

which did not hamper the (outermost) edge extraction. In contrast, the Canny edge detection filter works in a multi-stage process where initial smoothing of the image is achieved by using a low-pass Gaussian convolution filter, followed by the use of the derivative of the Gaussian filter for measuring the gradient of the image, then assigning edges to strong and weak categories by sensitivity threshold, and finally keeping the strong edges as well as only those weak edges which are connected to any strong edges (Boland and Murphy, 2001; Costa et al., 2013; 2014). In this study, the default value of the standard deviation (square root of two) was used for the Gaussian smoothing filter (Costa et al., 2014). High values for the sensitivity threshold were automatically extracted from the highest value of the gradient magnitude of the image (Costa et al., 2014), and 0.4 times the high threshold value was used as the lower threshold.

Othman et al. (2009) found that Canny edge extraction produced better edge detection results (thin and smooth edges) in medical images, whereas Kashyap et al. (2015) found better results in boundary extraction of a hand palm image with noise using the Sobel method with a median filter. In this study, the images in some places contain very small islands or exposed rocks near the larger islands. For instance, in Figure 4(a), portions of Chuja Island and nearby exposed rocks can be observed in the ENC-based coastline map. These very small islands or exposed rocks were found to be correctly identified by the Sobel edge extraction method (Figure 4(b)). In contrast, in the Canny edge detection method (Figure 4(c)) some non-land pixels along with the exposed rocks also became fused to the larger islands, because weak edges in the output are included while they are connected to strong edges (Boland and Murphy, 2001; Naz and Rao, 2014). Therefore, finally the Sobel edge detection method was selected to be used for edge extraction.

2.2.2. *Objects detection.* The broken lines detected in the previous step were thickened by dilating the pixels. Thus, closely located edge lines became connected which resulted in formation of many continuous lines on the object areas of which the outermost polygons represent the boundaries. This dilation of pixels also resulted in addition of a buffer zone around the outermost boundaries (for the current study, seven pixels towards the sea). Afterwards, the pixels inside the completed object boundaries were filled up by assigning value 1.0 (similar to that of the boundary pixel values). The changes in pixel values during some crucial steps of the proposed method are schematically presented in Figure 5. From Figure 5(a) it can be seen that all of the detected object pixels contain value 1, and rest of the pixels (black pixels containing value 0) represent sea.

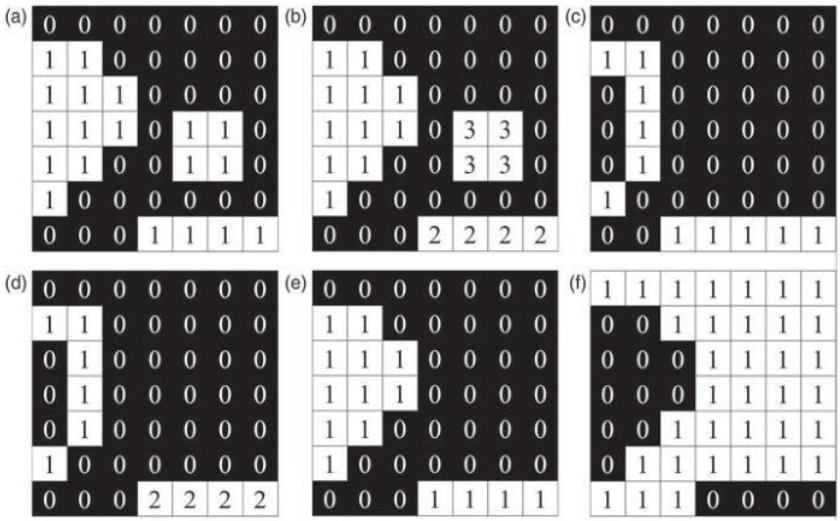

Figure 5. Schematic demonstration of changes in pixel values during some crucial steps of land masking: object detection (a), object labelling (b), ENC-based coastline (c), elimination of non-land object boundaries from (b) figure (d), retained land objects (e), and creating land mask (f).

2.2.3. *Geocorrection and object labelling.* Geocorrection was applied after detecting all of the objects in an image. It was accomplished using coordinates of the four corners of each image through constructing an affine spatial-referencing matrix. After geocorrection, detected areas were labelled separately. In the schematic example (Figure 5(b)) the detected three object pixels are labelled by three numbers from 1 to 3. For the purpose of the demonstration, it is assumed that the label 3 represents a ship (located near the centre of the image).

2.2.4. *ENC land area-based coastlines and other types of coastlines.* An ENC contains various types of hydrological data such as land area, coastlines, depths, etc, at very high resolution with global coverage. In this study, ENC-based land area map data was used to obtain the coastline map. The ENC land area (LNDARE) data are encoded as three types of objects, namely point, line and area objects (International Hydrographic Organization (IHO), 2014) from which the point-type data is used. ENC data (released by the Korea Hydrographic and Oceanographic Administration (KHOA), South Korea) was converted to the shape file format and used to extract coastline as polygons. However, for the observation of different coastal regions of the Korean Peninsula we used all six codes of KHOA provided ENCs (http://www.khoa.go.kr/eng/kcom/cnt/selectContentsPage.do?cntId=21050300).

The point-type geolocation information of shape files in the ENC was used to create binary maps similar to the coverage of respective geocorrected KOMPSAT-5 images. ENC coastlines cover coastline information of not only large islands but also very small islands, exposed rocks, sea stacks, etc. The superiority in delineation of very small islands and exposed rocks by an ENC over the freely available coastline data such as GSHHS (Wessel and Smith, 1996) is depicted in Figure 6 by superimposing those on Google Earth images

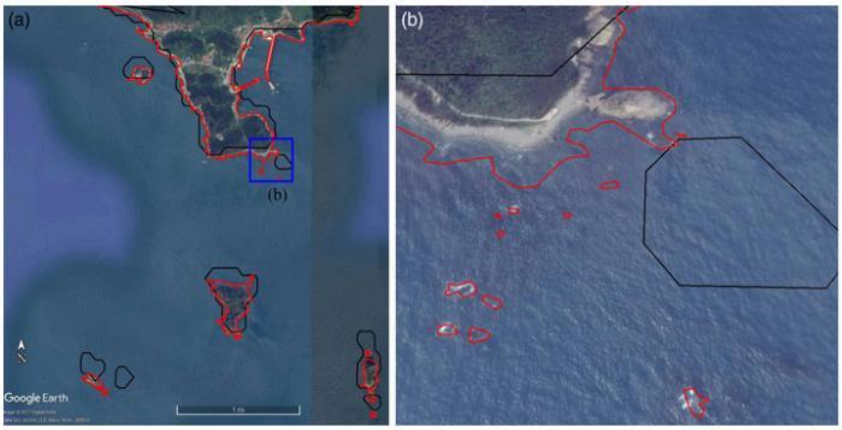

Figure 6. Suitability of ENC-based coastline (red polygons) over GSHHS-based coastline (black polygons) as presented by superimposing on Google Earth image (a) for ROI-1 (Figure 1). The enlarged image (b) for the blue box in (a) indicates mismatching for GSHHS-based coastline.

for the ROI-1 area (see Figure 1(b)). GSHHS is available in shape file format with a higher resolution mode developed and maintained by the University of Hawaii, and the National Oceanic and Atmospheric Administration (NOAA) Laboratory (Pelizzari, 2011). We used a Level 1 shape file for shoreline data which contains continental land masses and ocean island shoreline data. Very small obstacles just under the sea surface in the shallow areas may create noise in SAR images. However, using the ENC-based coastline map data only the land areas were masked out. Noticeably, very small rocks which could not be easily detected by other methods of land masking were also masked here, and depth data were also referred to in this process. For a better view, a small area (the blue rectangle) in Figure 6(a) is enlarged as Figure 6(b) from which it can be seen that in comparison to a Google Earth map, a few small exposed rocks in the southern parts of Chuja Island are also detected by the ENC-based coastline map, but not by the GSHHS map. Moreover, a small piece of land is detected as an isolated land mass with a shift towards the southeast. Therefore, in this study the ENC-based maps were used to delineate the land; small islands and exposed rocks were thus masked out properly. As the Sobel edge detection and ENC-based map is combined for land masking, hereafter in this manuscript the proposed method will be referred to as the Sobel-ENC method in order to differentiate it from other common methods of land masking.

2.2.5. *Elimination of non-land object labels.* The object-labelled images contained large islands, very small islands, exposed rocks and ships from which the large islands as well as small islands and exposed rocks need to be identified for land masking purposes. The ENC-based coastline comprises logically true data values only for coastline pixels. As the ships in the sea are not covered by the ENC-based coastline data, the object labelled image pixels were multiplied by the ENC-based image pixels in order to eliminate those non-land (ships) labels. In the schematically illustrated ENC-based coastline image (Figure 5(c)), the coastline pixels (white pixels with value 1) do not pass through the area of object number 3 (assumed to be a ship) in Figure 5(b). Thus, multiplying the

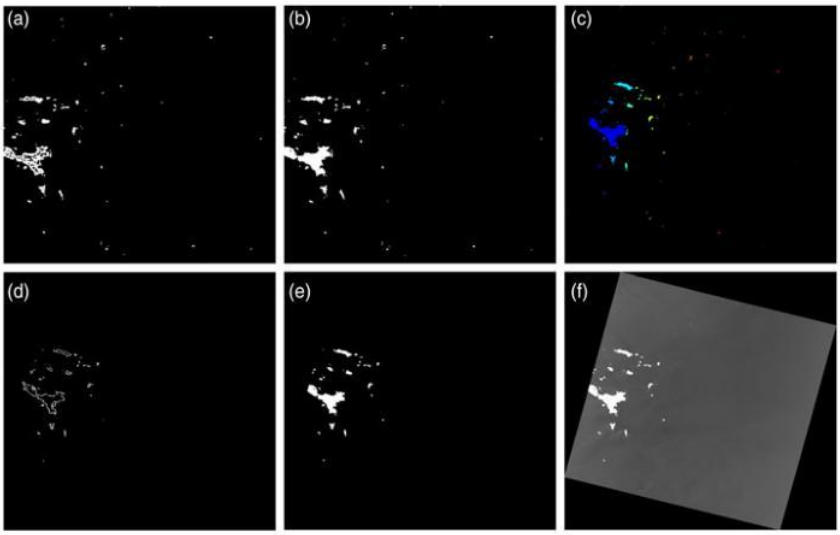

Figure 7. Application of TI-1 SAR image to land masking according to the procedure in Figure 3. The images obtained at each step are SAR edges (a), object detection (b), geocorrection and object labelling (c), ENC-based coastline (d), elimination of non-land object labels (e), and land masked image (f).

object labelled image by the ENC-based coastline image results in elimination of the non-land objects (label 3 in Figure 5(d)); thus only labels 1 and 2 are retained. Now these two retained labels' pixels in the object labelled image (Figure 5(b)) are converted to 1 as shown in Figure 5(e). For land masking purposes, the retained object pixel values were finally converted to 0, and the sea pixels were converted to 1 (Figure 5(f)).

2.3. *Application of Ship Detection Algorithm.* The KOMPSAT-5 images were geo-corrected again and the land areas including small islands and exposed rocks were masked out using the produced land mask image. Afterwards, a ship detection algorithm previously developed by the Laboratory for Satellite Oceanography & Marine Safety (LaSOMS), Marine Safety Research Center, KIOST, South Korea was applied to the land masked images. The algorithm takes land masked images as inputs and produces outputs as maps where the detected ships are shown as bordered and coloured objects, as well as saving the information of detected ships as a shape file format.

3. RESULTS AND DISCUSSION. Following the proposed Sobel-ENC method we obtained good results in land masking including masking of very small islands and exposed rocks. Though the proposed procedure was applied to the whole area of the two KOMPSAT-5 images, for better illustration the changes in ROI-1 area during the various steps of land masking are shown in Figure 7. From Figure 7(a) it can be seen that the broken lines are connected as created by applying Sobel edge extraction; thus, complete boundaries of all objects are obtained. In the following step, all of the objects are detected by filling up the areas inside object boundaries (Figure 7(b)). Next, geocorrection was applied, followed by labelling of the detected objects, as shown by assigning different colours (only for illustration purposes) to each of the objects in Figure 7(c). In

Figure 8. Comparison of KOMPSAT-5 based land areas (white patches) and ENC coastline (dark grey line) for ROI-1 (Figure 1).

Figure 7(d) the ENC-based coastline is shown where the lines representing coastlines are thickened for visualisation purposes. The image for land masking is prepared by discarding all of the labelled objects that are not crossed by an ENC coastline. This is done by multiplying the images of Figures 7(c) and 7(d) (changes in pixels values are schematically shown in Figure 5) which resulted in the extraction of only land objects such as large and small islands, and exposed rocks (Figure 7(e)); thus the non-land objects (shades of red and orange colours in Figure 7(c)) were appropriately eliminated. Finally, using retained object label information, the respective KOMPSAT-5 image was properly masked (Figure 7(f)).

For comparison purposes, ENC-based coastlines are superimposed on the detected objects image for the ROI-1 area (Figure 8). It can be clearly observed that three small objects at the south of the island in the centre of the image and the southernmost small object do not match with the ENC coastline. These objects were removed during the proposed method of land masking through multiplication of ENC by object labelled images (Figure 7(e)).

The results of land masking using different types of coastline maps for ROI-1 and ROI-2 are compared in Figures 9 and 10, respectively. Figures 9(a) and 10(a) show the geocorrected KOMPSAT-5 intensity images. From Figure 9(b) it can be seen that the proposed Sobel-ENC method has correctly masked out all land objects. Some speckle noise existed near the southern parts of larger land areas at the centre and south-eastern part of the Sobel method results (Figure 9(c)). When only an ENC map was used for land masking, some objects were not detected at the northern east corner of Chuja Island. In Figure 10 the black areas near the leftmost lower side of the images an outside of TI-2 coverage (refer to Figure 1(b)). It can be seen that the proposed Sobel-ENC method has detected the land (Figure 10(b)), but, in Figure 10(c) we can see that in the Sobel-only method many small

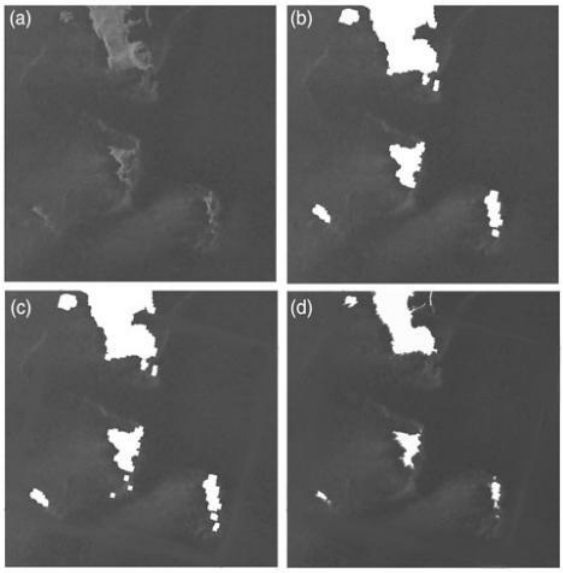

Figure 9. Land masking results for ROI-1 (Figure 1) using the geocorrected SAR intensity (a). Images (b), (c) and (d) represent Sobel-ENC method application, Sobel only method result, and ENC-based only product, respectively.

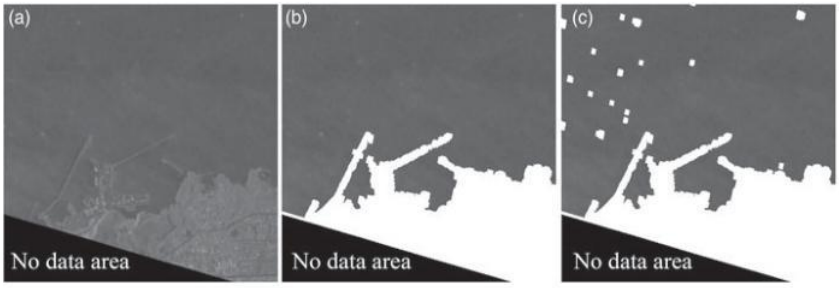

Figure 10. Land masking results for ROI-2 (Figure 1) using the geocorrected SAR intensity (a). Images (b) and (c) show Sobel-ENC method application and Sobel only method results, respectively.

objects still exist in the land mask image. Thus, the proposed Sobel-ENC method produced better land masking results.

The proposed method of land masking can also mask out newly constructed structures or renovation in existing construction. As an example, a bridge in Chuja Island is properly masked by our method (marked by small rectangle in Figure 11(a)) as well as detected in the ENC-based map (Figure 11(b)), but not detected in freely available GSHHS maps (Figure 11(c)). Similarly, construction of new breakwaters (marked by blue, red and green rectangles) can be observed in the Google Earth image (Figure 12(a)). Similar to the Google Earth image, all of the constructed breakwaters are also detected in our method

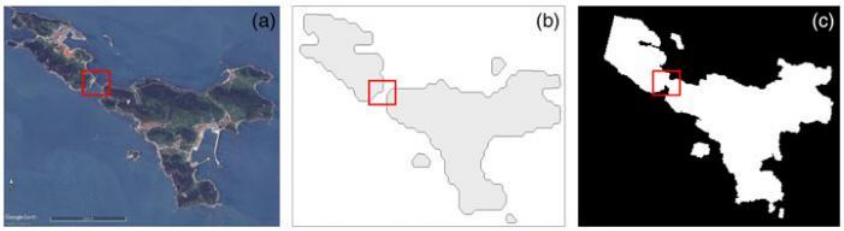

Figure 11. Validation of the land masking method for ROI-1 (Figure 1). The bridge in the red box of the Google Earth image (a), not covered by the GSHHS map (b), was classified into a man-made structure or land area (c).

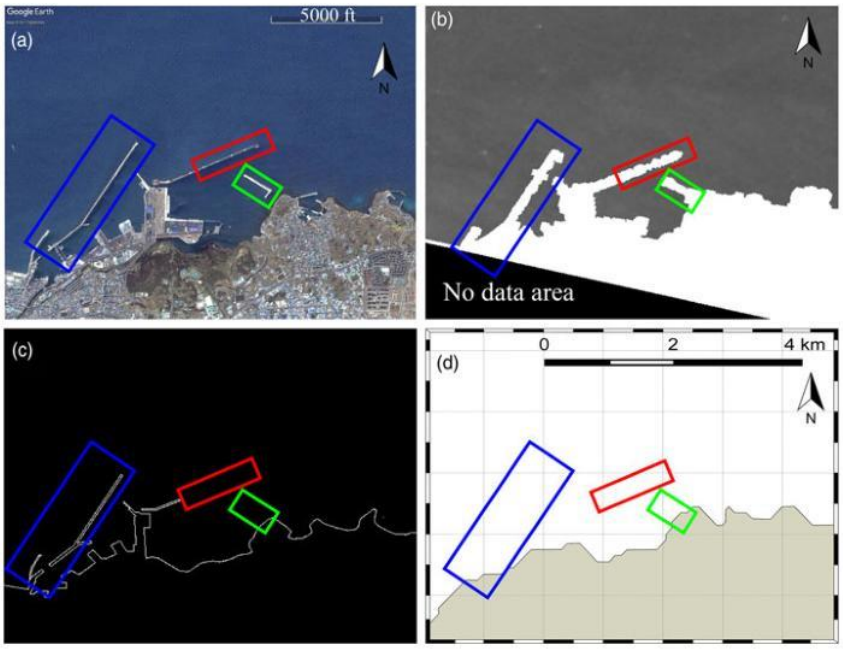

Figure 12. Validation of the land masking method for ROI-2 (Figure 1). Some recent changes in coastal constructions (inside colour rectangles), noticed in Google Earth image (a), are visible in the land masked image by proposed Sobel-ENC method (b), but not traced in ENC-based coastline map (c) and GSHHS (d).

(Figure 12(b)), though the portions of breakwaters marked by red and green rectangles were not included in the applied version of the ENC map (Figure 12(c)). In contrast, no breakwaters are covered by the GSHHS map (Figure 12(d)).

Finally, the masked images of TI-1 and TI-2 were used to detect ships automatically by applying the ship detection algorithm developed by KIOST. The results of ship detection for TI-1 and TI-2 are shown in Figures 13(a) and 13(b), respectively. From each image one smaller area is enlarged and shown at the right of each image. Google Earth images of

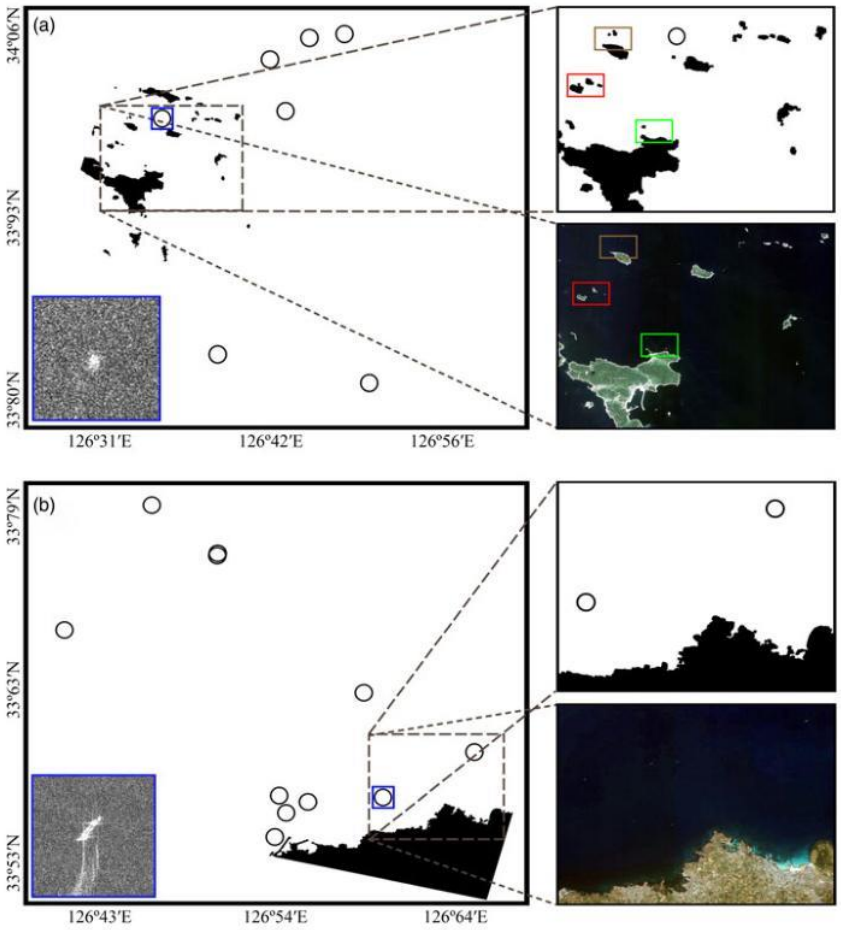

Figure 13. Ship detection results for TI-1 (a) and TI-2 (b) after applying the proposed land masking. The image inset shows a ship in a SAR intensity image (blue boxes in (a) and (b)). From each image one small area is projected (top right) and compared with the Google Earth image (bottom right). There are some discrepancies in the three coloured rectangles between two images that are caused by small rocks and shallow areas.

the same area are also placed at the bottom of the enlarged images. Figure 13(a) contains many small exposed rocks. Therefore, in both of the enlarged and Google Earth images of Figure 13(a), three small areas are bordered by three different colour rectangles to compare whether very small exposed rocks are also masked out through this process. Inside all rectangles of the ship detection result image, very small sea rocks are seen as masked land which are not clearly visible in the Google Earth map (only visible after much zooming). In spite of having small islands and exposed rocks none were detected as ships.

As the proposed method showed better results in ship detection through proper land masking for the TI-1 and TI-2 images, we finally applied the proposed Sobel-ENC method

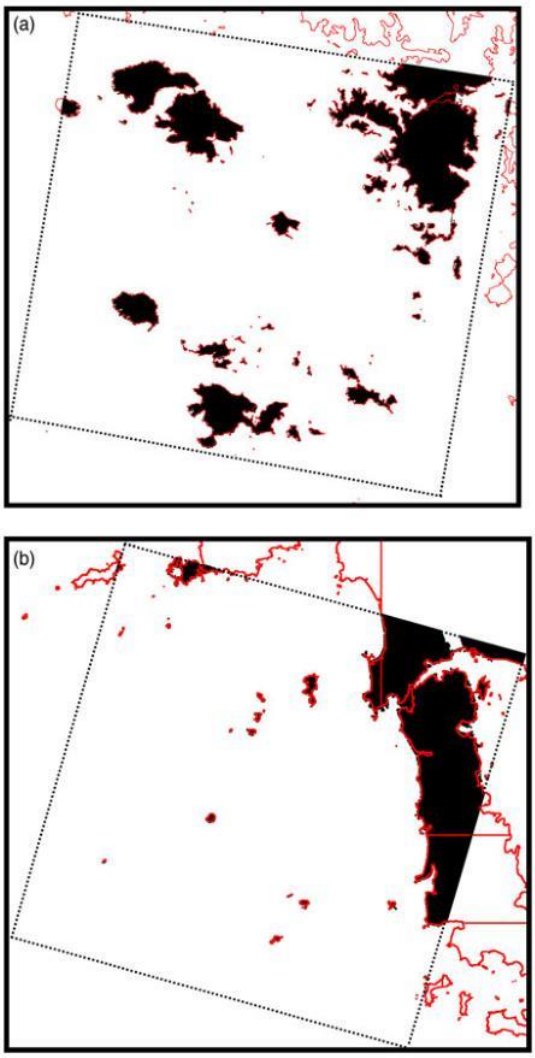

Figure 14. Land mask images for EI-1 (a), and EI-2 (b) with superimposed ENC-based coastlines (red lines).

to some other KOMPSAT-5 images. From those land masked images only two images, EI-1 and EI-2, which are geographically complicated (possessing many small islands and exposed rocks) are presented in Figure 14. Here, ENC-based coastlines (red lines) are also superimposed on the land masked image to check whether all of the land areas are correctly masked. It is observed that all of the land, including very small islands and exposed rocks, are also masked. Thus, the proposed method showed the ability to properly detect all land which matched with objects extracted from SAR images.

4. CONCLUSION. In this study, a new method of land masking for SAR images are proposed. The method is applied on KOMPSAT-5 images of different locations and periods. It is found that all land objects including the small islands and exposed rocks which were connected to land in the ENC can be successfully masked out through the proposed method. Moreover, this method can successfully detect newly developed structures such as bridges and breakwaters, as well as renovation in previously constructed structures better than when using freely available coastline data; thus performing better in ship detection when applying a ship detection algorithm. However, during coastline image preparation, small buffer zones were added to coastlines towards the sea which caused negligible error in land coverage. In general, it can be said that the proposed Sobel-ENC method produces better results in land masking than other methods, and can be applied on KOMPSAT-5 images for ship detection.

ACKNOWLEDGEMENTS

This research work is supported by the projects titled 'Development of Korea Operational Oceanographic System (KOOS), Phase 2', 'Development of Ship-handling and Passenger Evacuation Support System', and 'Construction of Ocean Research Stations and their Application Studies' funded by the Ministry of Oceans and Fisheries, Korea. The Authors greatly acknowledge the data support from Korea Aerospace Research Institute, South Korea.

REFERENCES

Al-amri, S. S., Kalyankar, N. V. and Khamitkar, S. D. (2010). Image Segmentation by using Edge Detection. *International Journal on Computer Science and Engineering*, **2**, 804–807.

Biamino, W., Borasi, M., Cavagnero, M., Croce, A., Di Matteo, L., Fontebasso, F., Tataranni, F. and Trivero, P. (2015). A "Dynamic" Land Masking Algorithm for Synthetic Aperture Radar Images. *Geoscience and Remote Sensing Symposium (IGARSS), 2015 IEEE International*, 4324–4327.

Boland, M. V. and Murphy, R. F. (2001). A Neural Network Classifier Capable of Recognizing the Patterns of all Major Subcellular Structures in Fluorescence Microscope Images of HeLa Cells. *Bioinformatics*, **17**(12), 1213–1223.

Brusch, S., Lehner, S., Fritz, T., Soccorsi, M., Soloviev, A. and van Schie, B. (2011). Ship Surveillance with TerraSAR-X. *IEEE Transactions on Geoscience and Remote Sensing*, **49**(3), 1092–1103.

Canny, J. (1986). A Computational Approach to Edge Detection. *IEEE Transactions on Pattern Analysis and Machine Intelligence*, **8**(6), 679–698.

Chaturvedi, S. K., Yang, C. S., Ouchi, K. and Shanmugam, P. (2012). Ship Recognition by Integration of SAR and AIS. *Journal of Navigation*, **65**(2), 323–337.

Costa, C., Antonucci, F., Boglione, C., Menesatti, P., Vandeputte, M. and Chatain, B. (2013). Automated Sorting for Size, Sex and Skeletal Anomalies of Cultured Seabass using External Shape Analysis. *Aquacultural Engineering*, **52**, 58–64.

Costa, C., Negretti, P., Vandeputte, M., Pallottino, F., Antonucci, F., Aguzzi, J., Bianconi G. and Menesatti, P. (2014). Innovative Automated Landmark Detection for Food Processing: The Backwarping Approach. *Food and Bioprocess Technology*, **7**(8), 2291–2298.

Della Rocca, M. R., Fiani, M., Fortunato, A. and Pistillo, P. (2004). Active Contour Model to Detect Linear Features in Satellite Images. *International Archives of Photogrametry, Remote Sensing and Spatial Information Sciences*, **35**(B3), 446–450.

Dellepiane, S., De Laurentiis, R. and Giordano, F. (2004). Coastline Extraction from SAR Images and a Method for the Evaluation of the Coastline Precision. *Pattern Recognition Letters*, **25**, 1461–1470.

Feng, J., Jiao, L. C., Zhang, X., Gong, M. and Sun, T. (2013). Robust Non-local Fuzzy C-means Algorithm with Edge Preservation for SAR Image Segmentation. *Signal Processing*, **93**(2), 487–499.

Gao, W., Zhang, X., Yang, L. and Liu, H. (2010). An Improved Sobel Edge Detection. In *Computer Science and Information Technology (ICCSIT), 2010 3rd IEEE International Conference on 2010 July 9*, **5**, 67–71.

Greidanus, H., Clayton, P., Indregard, M., Staples, G., Suzuki, N., Vachoir, P., Wackerman, C., Tennvassas, T., Mallorquí, J., Kourti, N. and Ringrose, R. (2004). Benchmarking Operational SAR Ship Detection. In *Proceedings of International Geoscience and Remote Sensing Symposium (IGARSS) 20–24 September 2004*, 4215–4218.

IHO. (2014). *Use of the Object Catalogue for ENC*, IHO Special Publication No. 57 (IHO S-57 Appendix B.1, Annex A), Edition 4.0.0, June, 2014, International Hydrographic Organization.

Jeong, H. G., Kotov, A. A. and Lee, W. (2013). A New Species of the Genus *Pleuroxus* Baird (Cladocera: Anomopoda: Chydoridae) from Jeju Island, South Korea. *Zootaxa*, **3666**(1), 31–40.

Jiang, Q., Wang, S., Ziou, D. and Zaart, A. (1999). Automatic Detection for Ship Targets in RADARSAT SAR Images from Coastal Regions. In *Vision Interface'99*, Trois-Tivieres, Canada, 131–137.

Karvonen, J. (2015). Evaluation of the Operational SAR Based Baltic Sea Ice Concentration Products. *Advances in Space Research*, **56**(1), 119–132.

Kashyap, Y., Vyas, A., Raghuwanshi, R. and Sharma R. (2015). Edge Detection using Sobel Method with Median Filter. *International Journal of Modern Trends in Engineering and Research*, **2**(5), 372–378.

Keramitsoglou, I., Cartalis, C. and Kiranoudis, C. T. (2006). Automatic Identification of Oil Spills on Satellite Images. *Environmental Modelling & Software*, **21**, 640–652.

Kim, T. H., Yang, C. S., Oh, J. H. and Ouchi, K. (2014). Analysis of the Contribution of Wind Drift Factor to Oil Slick Movement under Strong Tidal Condition: Hebei Spirit Oil Spill Case. *PLoS One*, **9**(1), e87393.

Kodors, S. and Zarembo, I. (2013). Urban Objects Segmentation using Edge Detection. *Environment. Technology. Resources. Proceedings of the 9th International Scientific and Practical Conference,* **1**(I). Rçzeknes Augstskola, Rçzekne, RA Izdevniecîba.

Krebs, G.D. (2017). "KOMPSAT 5 (Arirang 5)," Gunter's Space Page. http://space.skyrocket.de/doc_sdat/kompsat-5.htm. Accessed 22 February 2017.

Lee, S. R. (2010). Overview of KOMPSAT-5 Program, Mission, and System. *Geoscience and Remote Sensing Symposium (IGARSS), 2010 IEEE International*.

Liu, H. and Jezek, K. C. (2004). Automated Extraction of Coastline from Satellite Imagery by Integrating Canny Edge Detection and Locally Adaptive Thresholding Methods. *International Journal of Remote Sensing*, **25**(5), 937–958.

Margarit, G., Barba, J. A. and Tabasco, A. (2009). Operative Ship Monitoring System Based on Integrating AIS Polls within Synthetic Aperture Radar (SAR) Imagery. *WIT Transactions on the Built Environment*, **108**, 325–337.

Mashaly, A. S., AbdElkawy, E. F. and Mahmoud, T. A. (2014). Ship Detection in SAR Images using Efficient Land Masking Methods. *Society of Photo-optical Instrumentation Engineers (SPIE) Conference Series (Vol. 9093)*.

Montuori, A., Nunziata, F. and Migliaccio, M. (2010). A Multi-polarization Approach for SAR Ship Detection. *Proceedings of the XVIII RiNEm*. Benevento.

Naz, S. and Rao, S. N. (2014). Glaucoma Detection in Color Fundus Images using Cup to Disc Ratio. *The International Journal of Engineering and Science*, **3**, 51–58.

Othman, Z., Haron, H. and Kadir, M. R. A. (2009). Comparison of Canny and Sobel Edge Detection in MRI Images. *Computer Science, Biomechanics & Tissue Engineering Group, and Information System*, 133–136.

Pelizzari, S. A. (2011). Oil Spill Detection using SAR Images. *Doctoral dissertation, Instituto Superior Técnico, Universidade Tecnica de Lisboa*, Lisbon, Portugal.

Ramadevi, Y., Sridevi, T., Poornima, B. and Kalyani, B. (2010). Segmentation and Object Recognition using Edge Detection Techniques. *International Journal of Computer Science & Information Technology*, **2**, 153–160.

Romeiser, R., Breit, H., Eineder, M., Runge, H., Flament, P., De Jong, K. and Vogelzang, J. (2005). Current Measurements by SAR Along-track Interferometry from a Space Shuttle. *IEEE Transactions on Geoscience and Remote Sensing*, **43**(10), 2315–2324.

Senthilkumaran, N. and Rajesh, R. (2009). Edge Detection Techniques for Image Segmentation- A Survey of Soft Computing Approaches. *International Journal of Recent Trends in Engineering*, **1**, 250–254.

Shahane, P. R., Choukade, A. S. and Diyewar, A. N. (2015). Online Signature Recognition using MATLAB. *International Journal of Innovative Research in Electrical, Electronics, Instrumentation, and Control Engineering*, **32,** 107–112.

Shu, Y., Li, J., Yousif, H. and Gomes, G. (2010). Dark-spot Detection from SAR Intensity Imagery with Spatial Density Thresholding for Oil-spill Monitoring. *Remote Sensing of Environment*, **114**(9), 2026–2035.

SI Imaging Services. (2015). KOMPSAT-5 Product Specifications- Standard Products Specifications. Version 1.2. Korea Aerospace Research Institute. http://www.si-imaging.com/wp-content/uploads/2016/12/KOMPSAT-5_Standard_Products_Specifications_v1.2.pdf. Accessed 27 February 2017.

Simpson, J. J. (1990). On the Accurate Detection and Enhancement of Oceanic Features Observed in Satellite Data. *Remote Sensing of Environment*, **33**(1), 17–33.

Singh, E. H. and Kaur, E. T. (2013). Implementation of Various Edge Detection Techniques for Gray Scale Images in VC++. *International Journal of Emerging Technologies in Computational and Applied Sciences*, **6**(4), 280–284.

Slater, J. A., Garvey, G., Johnston, C., Haase, J., Heady, B., Kroenung, G. and Little, J. (2006). The SRTM data finishing process and products. *Photogrammetric Engineering & Remote Sensing*, **72** (3), 237–247.

Sobel, E. C. (1990). The Locust's use of Motion Parallax to Measure Distance. *Journal of Comparative Physiology A: Neuroethology, Sensory, Neural, and Behavioral Physiology*, **167**(5), 579–588.

Trivero, P., Adamo, M., Biamino, W., Borasi, M., Cavagnero, M., De Carolis, G., Di Matteo, L., Fontebasso, F., Nirchio, F. and Tataranni, F. (2016). Automatic Oil Slick Detection from SAR Images: Results and Improvements in the Framework of the PRIMI Pilot Project. *Deep Sea Research Part II: Topical Studies in Oceanography*, **133**, 146–158.

Wall, C. C., Muller-Karger, F. E., Roffer, M. A., Hu, C., Yao, W. and Luther, M. E. (2008). Satellite Remote Sensing of Surface Oceanic Fronts in Coastal Waters off West-central Florida. *Remote Sensing of Environment*, **112**(6), 2963–2976.

Wessel, P. and Smith, W. H. F. (1996). A Global Self-consistent, Hierarchical, High-resolution Shoreline Database. *Journal of Geophysical Research*, **101**, 8741–8743.

Yang, C. S. and Ouchi, K. (2008). Comparison of Ship Detectability using SAR Polarization Data: ENVISAT ASAR AP Mode. *Geoscience and Remote Sensing Symposium, 2008. IGARSS 2008. IEEE International, (Vol. 1). IEEE.*

Zhang, J. Y., Yan, C. and Huang, X. X. (2009). Edge Detection of Images Based on Improved Sobel Operator and Genetic Algorithms. In *Image Analysis and Signal Processing, 2009. IASP 2009. International Conference on 2009 April 2011*, 31–35.

Korean Journal of Remote Sensing, Vol.33, No.4, 2017, pp.437~444
http://dx.doi.org/10.7780/kjrs.2017.33.4.9

ISSN 1225-6161 (Print)
ISSN 2287-9307 (Online)

Article

Land Masking Methods of Sentinel-1 SAR Imagery for Ship Detection Considering Coastline Changes and Noise

Jeongju Bae* and Chan-Su Yang*†

* Maritime Safety Research Center, Korea Institute of Ocean Science and Technology

Abstract : Since land pixels often generate false alarms in ship detection using Synthetic Aperture Radar (SAR), land masking is a necessary step which can be processed by a land area map or water database. However, due to the continuous coastline changes caused by new port, bridge, etc., an updated data should be considered to mask either the land or the oceanic part of SAR. Furthermore, coastal concrete facilities make noise signals, mainly caused by side lobe effect. In this paper, we propose two methods. One is a semi-automatic water body data generation method that consists of terrain correction, thresholding, and median filter. Another is a dynamic land masking method based on water database. Based on water database, it uses a breadth-first search algorithm to find and mask noise signals from coastal concrete facilities. We verified our methods using Sentinel-1 SAR data. The result shows that proposed methods remove maximum 84.42% of false alarms.

Key Words : Land Masking, Sentinel-1, Ship Detection, Synthetic Aperture Radar

1. Introduction

Spaceborne Synthetic Aperture Radar (SAR) based ship detection is useful because SAR can collect ocean observation regardless time and weather (Matsuoka and Yamazaki, 2004; Ouchi, 2010). SAR ship detection consists of several image processing techniques where land masking is a necessary step because land is not a region of interest (ROI) and can generate false alarms (Crisp, 2004).

There are many studies about land masking. Crisp (2004) describes the water database based approach in his work, and Biamino *et al.* (2015) used Canny edge detection (Canny, 1986). However, Hwang *et al.* (2017) mentioned that water database is often different from the real world, omitting new port, bridge, reclaimed land built after the data published. For example, Busan New Port, a significant portion of Jeju Port and Geoga Bridge in South Korea are not covered by Shuttle Radar Topography Mission Water Body Data (NASA, 2003). Moreover, adjacent to land there are noise signals which are mainly caused by side lobe

Received December 29, 2016; Revised February 13, 2017; Accepted August 22, 2017.

† Corresponding Author: Chan-Su Yang (yangcs@kiost.ac.kr)

effect in Sentinel-1 SAR data. Hwang *et al.* (2017) mentioned that these problems cause false alarms. Although Canny method (1986) can solve these issues, it requires complex processing procedure, demanding a long computational time. Therefore, in this paper, we propose land masking methods of Sentinel-1 SAR imagery for improving ship detection accuracy. Then apply suggested methods to Sentinel-1 SAR data, and verify how many false alarms are eliminated.

2. Dataset

1) Sentinel-1 Synthetic Aperture Radar

The study area is Jeju Island, South Korea. Among the Jeju Island's location, we mainly focus on Jeju Port. As mentioned in the introduction, a significant portion of Jeju Port is not included in Shuttle Radar Topography Mission Water Body Data (SWBD). Therefore, we considered this place for the verification of the proposed method.

The Sentinel-1 mission is a constellation of two satellites of Sentinel-1A and Sentinel-1B which were launched in April 2014 and April 2016, respectively. Sentinel-1 satellites collect earth observation using C-band microwave SAR sensor. We used Sentinel-1B Level-1 Ground Range Detected (GRD) data to make new water body data for the verification purpose.

Table 1. Characteristics of Sentinel-1B SAR image used in this study

Satellite	Sentinel-1B
Location	Jeju Island
Date	October 9 2016, 21:32:36 (UTC)
Product Type	Level-1 Ground Range Detected
Acquisition Mode	Interferometric Wide Swath
Polarization	VH
Resolution	20 m × 22 m (Range × Azimuth)
Pixel Spacing	10 m × 10 m (Range × Azimuth)
Number of looks	5 × 1
Incidence Angle	30.72 ° ~ 46.14 °

Table 2. Characteristics of SWBD

	SRTM Water Body Dataset
Publication year	2003
Coverage	56 ° S ~ 60 ° N
Resolution	1 arc second (≈ 30 m)
Projection	Geographic

Table 1 shows the characteristics of the Sentinel-1B imagery used in this study.

Since Sentinel-1 uses Terrain Observation with Progressive Scans SAR (TOPSAR) techniques, side lobe effect often appears (Piantanida, 2016). Moreover, the spatial resolution of Sentinel-1 GRD image is different from pixel spacing. These characteristics make the land masking imprecise.

2) Shuttle Radar Topography Mission Water Body Dataset

The Shuttle Radar Topography Mission Water Body Dataset (SWBD) is a set of high-resolution (1 arc-second) water database published by NASA, 2003. It is the level-2 product of SRTM Digital Terrain Elevation Data. Table 2 shows the characteristics of the SWBD. Since the publication year is 2003, it does not describe landfills, bridges and new port built after 2003.

3. Method

1) Preprocessing

Preprocessing is applied in advance to semi-automatic water body data generation or ship detection. This stage consists of radiometric calibration and geometric correction. Geometric correction is necessary because Sentinel-1 SAR image has geometric distortion. We use Range-Doppler geocoding method to correct data (Small and Schubert, 2008). Bayanudin and Jatmiko (2016) reported Range-Doppler geocoding has about 25 m (≈ 2.5 pixels) of root mean square error.

Since Range-Doppler geocoding requires a radiometrically calibrated image, radar reflectivity is transformed into radar cross-section before the Range-Doppler geocoding.

2) Semi-automatic Water Body Data Generation

After the preprocessing stage, the proposed method begins to generate water body data semi-automatically. Usually, the land intensity is higher than the ocean. Thus thresholding briefly classifies land and ocean. In this work, the threshold value is determined automatically based on statistical method. First, intensity histogram of target data is constructed by counting the pixel intensity where elevation is higher than 50 m. We use General Bathymetric Chart of the Oceans (GEBCO) to get pixel elevation. Since the histogram only counts the pixel which elevation is higher than 50 m, it only counts land pixels. Then find bottom x% value of land intensity using the histogram, and set as the threshold value. Afterwards, thresholding is applied. It is expected that this stage masks out (100-x)% of land pixels. Since ocean intensity usually much lower than the land, most ocean pixels remain in this step. After that, median filtering is repeated to fill the hole or remove the noise. Finally, manual correction is applied. Fig. 1 shows the flowchart of semi-automatic water body data generation from Sentinel-1 SAR image.

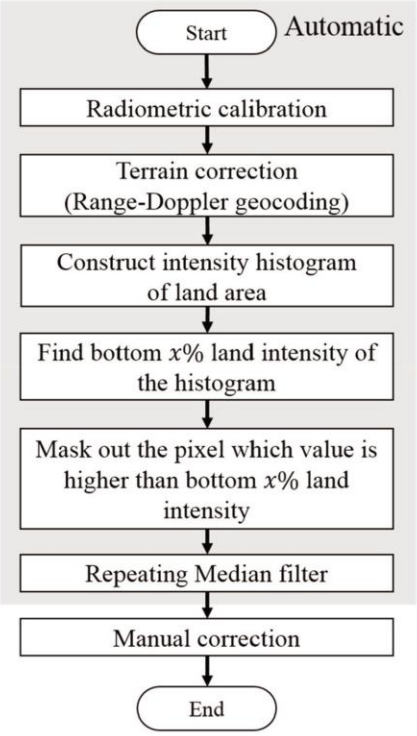

Fig. 1. Flowchart of semi-automatic water body data generation. The gray portion represents an automated part.

3) Breadth-First Search Applied Land Masking

Usually, the noise adjacent to the land, especially side lobe, is continuous to the land and has high intensity compared to the ocean. Thus breadth-first search (BFS) can be used for finding and masking the noise pixels. It is a kind of algorithm to traversing the graph or matrix. Since raster image can be interpreted as pixel matrix (Silvela and Portillo, 2001), BFS can traverse the noise pixels from land pixels.

For the proposed BFS applied land masking method first, intensity of 4-direction neighboring of the land pixels, which determined by water database, are investigated. Then, select the pixels which intensity is higher than the threshold. After that, invest and choose the neighborhood pixels from the selected pixels again. This neighboring pixels selection is repeated until no more pixel is selected or BFS reaches the maximum depth. Finally, mask out all selected pixel. In this method, configuring maximum BFS depth is critical to protecting mask out too many pixels. We used 20 pixels as the maximum depth. Fig. 2 shows the visual explanation of the proposed method.

The intensity statistics of target Sentinel-1 data is summarized in Table 3. The land intensity is about 3.5

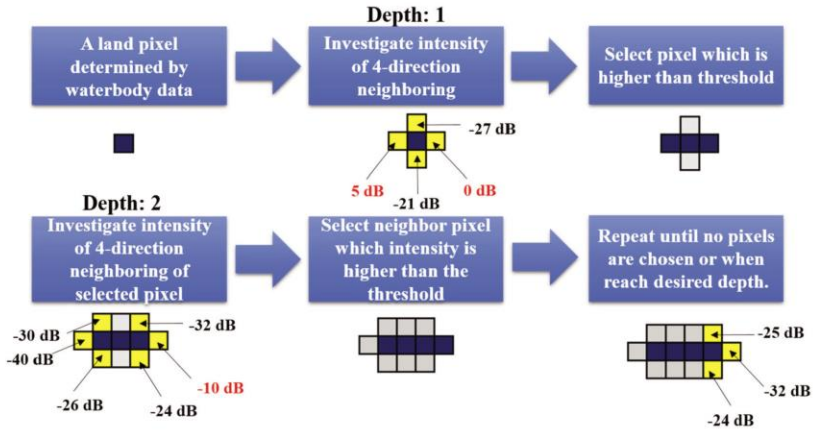

Fig. 2. A visual explanation of breadth-first search traversing. Deep blue represents chosen pixel which will be masked out, yellow represents neighbor pixels of chosen pixel, and gray represents the neighbor pixels which are classified as ocean pixels. In this example, -15 dB is a used as a threshold.

Table 3. Intensity statistics of study area

Unit: Radar cross section (Sigma nought)	Land intensity	Ocean intensity
Mean	0.0357	0.0019
Median	0.0561	0.0067
Top 5% value	0.75945142	0.00938210
Bottom 5% value	0.03371320	0.00078379

times higher than top 5% of the ocean intensity. Hence, we used top 5% ocean intensity as a threshold.

4) Ship Detection

We used moving average constant false alarm rate (CFAR) detector as a prescreening stage in ship detection because it is simple, fast, and most commonly adopted algorithm (Crisp, 2004). CFAR detector commonly uses Gaussian distribution as a statistical model (Crisp, 2004). Therefore, we applied Gaussian distribution to our CFAR detector. After the prescreening stage, the discrimination stage began. Many ship detection implementations have a discrimination stage after prescreening to reduce false alarms (Crisp, 2004). We used contours finding technique (Shaw, 2015) as discrimination stage. This technique is composited with Canny edge detection (Canny, 1986) and structural analysis method (Suzuki, 1985). In the Sentinel-1 image, it is difficult to distinguish objects less than 20 m in size. Therefore, the discrimination stage excludes all object which length is shorter than 20 m.

4. Result

Fig. 3(a) is the Sentinel-1 GRD intensity image used in this study. Fig. 3(b) shows Jeju Port and Fig. 3(c) is SWBD of Jeju Port.

1) Semi-Automatic Water Body Data Generation

Fig. 4 shows the threshold result of the semi-automatic water body data generation. In Fig. 4(a), the threshold value is low; thus many ocean pixels are masked out. On the contrary, in Fig. 4(b) and Fig. 4(c), fewer ocean pixels are incorrectly masked out whereas more pixels on the land remains unmasked.

Fig. 5 is the result of the median filter to Fig. 4(b). The image showed in Fig. 5(a) is produced when the

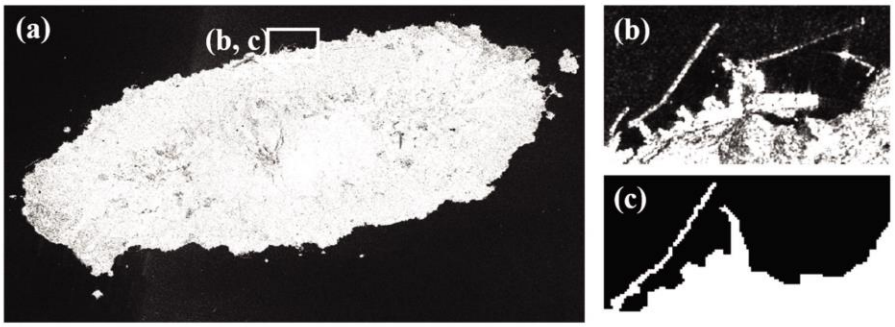

Fig. 3. (a) Sentinel-1 GRD intensity image of Jeju Island where the area for Jeju Port is selected as Region of Interest (ROI) and marked by a small rectangle which is projected as (b). The Shuttle Radar Topography Mission Water Body Data for the ROI is shown in (c).

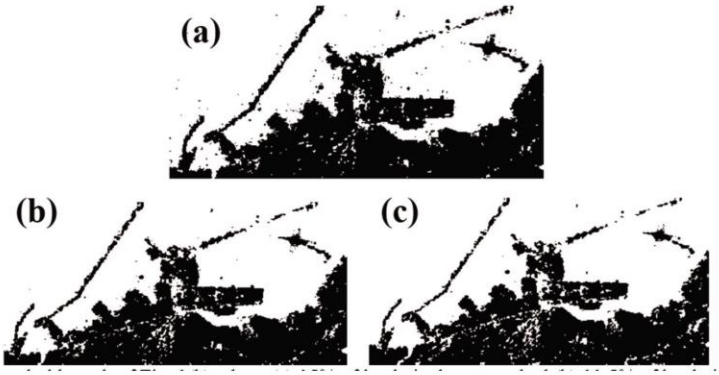

Fig. 4. Threshold result of Fig. 3(b) where (a) 95% of land pixels are masked (b) 92.5% of land pixels are masked (c) 90% of land pixels are masked. In the images, dark portions indicate masked area.

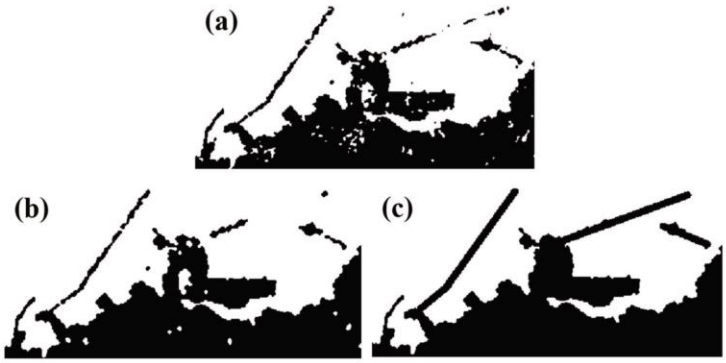

Fig. 5. (a) Median filter applied to Fig. 4(b); (b) 15 times median filter repeated; and (c) Manual correction of (b).

median filter is applied only once. Fig. 5(b) shows the result when the median filter is applied 15 times, and it shows better result compared to Fig. 5(a). Repeating median filter more than 15 times almost has no additional effect; thus not followed in this study. Due to the information loss during the thresholding and median filtering, we have manually corrected the semi-automatically generated data (the result of Fig 5(b)) as shown in Fig. 5(c).

2) Land Masking Result and Evaluation

Fig. 6 shows land masking result of each water body data and proposed method. Jeju Port remains when SWBD is used. Contrary to the Fig. 6(a), Jeju Port is masked out in Fig 6(b) and Fig. 6(c) which are the result of proposed methods.

Fig. 7 shows ship detection result of Fig. 6. In Fig. 7(a) there are lots of false alarms. Contrary to Fig. 7(a), Fig. 7(b) has less false alarms. Even, Fig. 7(c) does not show any false alarm.

Table 4 summarizes ship detection result of Fig. 3(a),

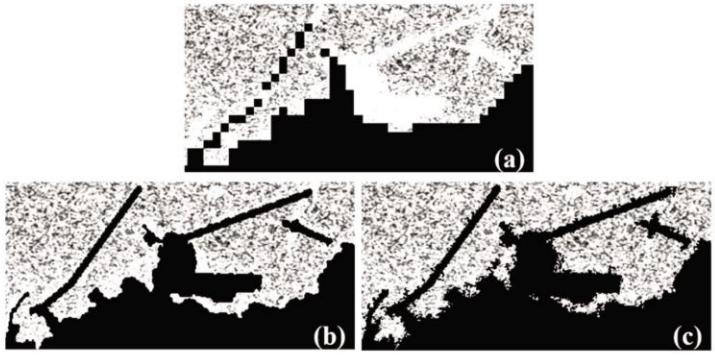

Fig. 6. Land masking results of the Jeju Port using (a) SWBD (b) semi-automatically generated water body data (c) semi-automatically generated water body data, and breadth-first search based method applied.

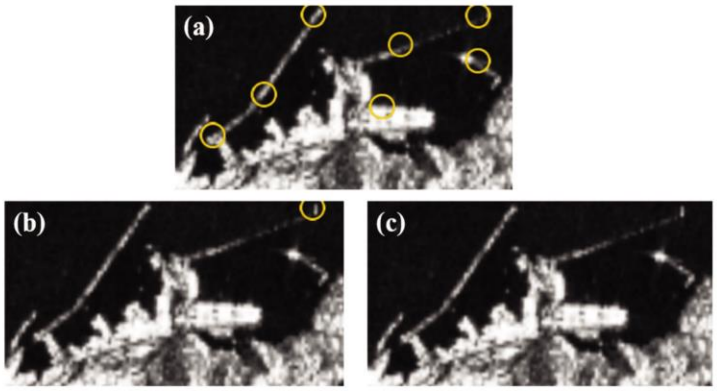

Fig. 7. Ship detection result of Fig. 6. Yellow circle represents detected object. (a) Ship detection result of Fig. 6(a). Many false alarms detected. (b) Ship detection result of Fig. 6(b). Most false alarms are removed. (c) Ship detection result of Fig. 6(c). No false alarm is found.

Table 4. Ship detection result of Fig. 3(a)

Dataset and land masking method	SWBD	Semi-automatically generated water body data	Semi-automatically generated water body data + BFS method
Detected object	227	113	91
False alarm	154	46	24
Ratio: False alarm / detected object	67.84%	40.71%	26.37%
Relative false alarm rate to SWBD	–	29.87%	15.58%

not Jeju Port but the whole area of Jeju Island. We use CFAR detector and contours finding technique to land eliminated data. Semi-automatically generated water body data generates 46 false alarms, and additional BFS applied land masking method generates 24 false alarms while SWBD based land masking generates 154 false alarms. Consequently, proposed methods reduce maximum 84.42% of false alarms.

5. Conclusion

Since water body data such as SWBD does not describe the recent geographic change, ship detection often generates numerous false alarms. Moreover, the noise such as side lobe also generates false alarms. In this paper, we propose semi-automatic water body data generation and BFS applied land masking method. Our methods uses terrain correction, thresholding, median filter for semi-automatic water body data generation and breadth-first search for mask out noises. The experiment shows that our methods remove maximum 84.42% of false alarms in target Sentinel-1 SAR data.

Further study will include the utilization of bathymetry data for land masking and measurement of side lobe effect to improve our work.

Acknowledgment

This research is a part of the projects entitled "Remote Sensing Surveillance System for Supporting Illegal, Unreported and Unregulated (IUU) Fishing Control Activities" and "Cooperative Project on Korea-China Bilateral Committee on Ocean Science" by the Ministry of Oceans and Fisheries, Korea and China-Korea Joint Ocean Research Center, and also based on work supported by the Ministry of Oceans and Fisheries under Maritime Safety and Transportation Facility Technology Development, "Development of Ship-handling and Passenger Evacuation Support System."

References

Bayanudin, A. A. and R. H. Jatmiko, 2016. Orthorectification of Sentinel-1 SAR (Synthetic Aperture Radar) Data in Some Parts Of South-eastern Sulawesi Using Sentinel-1 Toolbox, *IOP Conference Series: Earth and Environmental Science*, 47(1).

Biamino, W., M. Borasi, M. Cavagnero, A. Croce, L. Di Matteo, F. Fontebasso, F. Tataranni, and P. Trivero, 2015. A "dynamic" land masking algorithm for synthetic aperture radar images, *Proc. of 2015 International Geoscience and Remote Sensing Symposi*um, Milan, Italy, July 26-31, pp. 4324-4327.

Canny, J., 1986. A computational approach to edge detection, *IEEE Transactions on pattern analysis and machine intelligence* 6: 679-698.

Crisp, D. J., 2004. *The state-of-the-art in ship detection in synthetic aperture radar imagery*, Defence Science and Technology Organisation Salisbury Info Sciences Lab, Australia.

Hwang, J., D. Kim, and H.-S. Jung, 2017. An Efficient Ship Detection Method for KOMSAT-5 Synthetic Aperture Radar Imagery based on Adaptive Filtering Approach, *Korean Journal of Remote Sensing*, 33(1): 89-95.

Matsuoka, M. and F. Yamazaki, 2004. Use of Satellite SAR Intensity Imagery for Detecting Building Areas Damaged Due to Earthquakes, *Earthquake Spectra*, 20(3): 975-994.

NASA, 2003. SRTM Water Body Data Product Specific Guidance, https://dds.cr.usgs.gov/srtm/version2_1/SWBD/SWBD_Documentation/SWDB_Product_Specific_Guidance.pdf.

Ouchi, K., 2010. *Principles of Synthetic Aperture Radar for Remote Sensing*, Dasom Publications, Busan, South Korea.

Piantanida, R., 2016. *Sentinel-1 Level 1 Detailed Algorithm Definition*, European Space Agency, Paris, France.

Shaw, D., 2015. Finding Contours in Images with OpenCV, http://www.codepool.biz/opencv-finding-image-contours.html.

Silvela, J. and J. Portillo, 2001. Breadth-first search and its application to image processing problems, *IEEE Transactions on Image Processing*, 10(8): 1194-1199.

Small, D. and A. Schubert, 2008. *Guide to ASAR geocoding*, University of Zurich, Zurich, Swiss.

Suzuki, S., 1985. Topological structural analysis of digitized binary images by border following, *Computer vision, graphics, and image processing*, 30(1): 32-46.